Earth Syst. Sci. Data, 15, 2153–2177, 2023
https://doi.org/10.5194/essd-15-2153-2023

Open Access Earth System Science Data

Fire weather index data under historical and shared socioeconomic pathway projections in the 6th phase of the Coupled Model Intercomparison Project from 1850 to 2100

Yann Quilcaille[★], Fulden Batibeniz[★], Andreia F. S. Ribeiro, Ryan S. Padrón, and Sonia I. Seneviratne

Institute for Atmospheric and Climate Science, Department of Environmental Systems Science, ETH Zurich, Zurich, Switzerland
★These authors contributed equally to this work.

Correspondence: Yann Quilcaille (yann.quilcaille@env.ethz.ch) and Fulden Batibeniz (fulden.batibeniz@env.ethz.ch)

Received: 28 November 2022 – Discussion started: 30 November 2022
Revised: 3 April 2023 – Accepted: 24 April 2023 – Published: 30 May 2023

Abstract. Human-induced climate change is increasing the incidence of fire events and associated impacts on livelihood, biodiversity, and nature across the world. Understanding current and projected fire activity together with its impacts on ecosystems is crucial for evaluating future risks and taking actions to prevent such devastating events. Here we focus on fire weather as a key driver of fire activity. Fire weather products that have a global homogenous distribution in time and space provide many advantages to advance fire science and evaluate future risks. Therefore, in this study we calculate and provide for the first time the Canadian Fire Weather Index (FWI) with all available simulations of the 6th phase of the Coupled Model Intercomparison Project (CMIP6). Furthermore, we expand its regional applicability by combining improvements to the original algorithm for the FWI from several packages. A sensitivity analysis of the default version versus our improved version shows significant differences in the final FWI. With the improved version, we calculate the FWI using average relative humidity in one case and minimum relative humidity in another case. We provide the data for both cases while recommending the one with minimum relative humidity for studies focused on actual FWI values and the one with average relative humidity for studies requiring larger ensembles. The following four annual indicators, (i) maximum value of the FWI (*fwixx*), (ii) number of days with extreme fire weather (*fwixd*), (iii) length of the fire season (*fwils*), and (iv) seasonal average of the FWI (*fwisa*), are made available and are illustrated here. We find that, at a global warming level of 3 °C, the mean fire weather would increase on average by at least 66 % in duration and frequency, while associated 1-in-10-year events would approximately triple in duration and increase by at least 31 % in intensity. Ultimately, this new fire weather dataset provides a large ensemble of simulations to understand the potential impacts of climate change spanning a range of shared socioeconomic narratives with their radiative forcing trajectories over 1850–2100 at annual and 2.5° × 2.5° resolutions. The produced full global dataset is a freely available resource at https://doi.org/10.3929/ethz-b-000583391 (Quilcaille and Batibeniz, 2022) for fire danger studies and beyond, which highlights the need to reduce greenhouse gas emissions for reducing fire impacts.

Published by Copernicus Publications.

1 Introduction

Anthropogenic climate change tends to make fires less predictable and exacerbate their impacts (Anon, 2019; Sanderson and Fisher, 2020). The Sixth Assessment Report of the Intergovernmental Panel on Climate Change (IPCC AR6) concluded that fire weather has become more widespread, longer-lasting, and more intense compared to preindustrial periods in some regions (e.g., the Mediterranean) and that these changes are expected to increase with higher global warming levels (Seneviratne et al., 2021). This is generally associated with an increased occurrence of concurrent hot and dry conditions with increasing global warming (Seneviratne et al., 2021). Unfortunately, we have already suffered several damaging wildfires in recent years throughout the world (e.g., Australia, Turkey and Greece, Siberia, Sweden, Canada, USA), with some of them formally attributed to human-induced climate change (Li et al., 2019; van Oldenborgh et al., 2021). Fires are not only destructive, but also release carbon stored in vegetation and thereby increase atmospheric CO_2 concentration (Lasslop et al., 2020). For example, released CO_2 emissions from 2019–2020 wildfires in Australia were at least higher than 35 % of the country's annual amount (Li et al., 2021; van der Velde et al., 2021).

Fire weather is defined as those conditions conducive to the occurrence and sustenance of fires, and it is characterized by compound hot, dry, and windy events. These conditions are increasing in frequency and intensity across many regions due to anthropogenic climate change (Abatzoglou et al., 2019; Ranasinghe et al., 2021; Seneviratne et al., 2021). Further increases in greenhouse gas forcing are likely to increase the occurrence of these compound conditions, favoring the occurrence of extreme events of fire emissions and burned area (Li et al., 2021; Jones et al., 2022; Ribeiro et al., 2022), more fire-prone regions, and more complex fire dynamics. It can also induce preconditions that can exacerbate the impacts of fire, such as tree mortality (Stevens-Rumann et al., 2012) and fuel accumulation (Marlon et al., 2009).

In addition to fire weather, human activities affect fires in multiple ways. On the one hand, agricultural expansion and landscape fragmentation caused by humans make the vegetation less flammable and create a decreasing trend in satellite observations (Jolly et al., 2015; Andela et al., 2017). On the other hand, human influence increases the fire risk in some regions due to negligence or arson. For example, the use of fire as a land-clearing tool for agriculture and deforestation may ignite uncontrollable wildfires and burn large forested areas, particularly during compound dry and hot events in regions such as the Amazon (e.g., Libonati et al., 2022; Ribeiro et al., 2022). At the same time, the most disastrous wildfires occur in wildland and urban transition areas, where the human effect is the largest (Bowman et al., 2017). Even though these dynamics are hard to investigate in a future climate, it is necessary and requires projected land-use transition and socioeconomic scenarios.

Historical fire weather can be investigated with observations, remote-sensing products, or more spatially and temporally homogeneous reanalysis datasets (Vitolo et al., 2019). Some of these datasets cover decades and allow longer statistical analysis. For example, fire season duration is increasing according to recent long-term satellite observations (Jolly et al., 2015). However, future fire activity is an enigma given the potential changes in ecosystems due to climate change and human activities. The interactions of human influence and climate change with fire dynamics are so complex that each ecosystem must be studied in its own right. Therefore, improvements to fire indices and a better understanding of the interactions between mean climate, climate extremes, humans, and fire are required to project future fire activity and to mitigate its consequences.

Several indicators of fire weather have been proposed over the years (Table A1). Although all of them have been developed to inform about fire risk, each one responded to different needs. Here, we focus on the Fire Weather Index (FWI) from the Canadian Forest Fire Danger Rating System (Van Wagner, 1987) for several reasons. First, this index represents potential fire danger rather than actual fire occurrence, only seizing how fire activity is prone according to meteorological conditions. The four major drivers of fire weather at a global scale (temperature, precipitation, relative humidity, and wind speed) are accounted for, also through the impact of the moisture content of potential fuel on the fire intensity. The second reason is that clear relationships have been shown between the FWI and the burned area in Earth system models (ESMs) (Bedia et al., 2015; Abatzoglou et al., 2018; Grillakis et al., 2022; Jones et al., 2022), making this index relevant for impact assessments. Finally, this index can be used at a global scale (Field et al., 2015) for fire danger predictability and warning systems (de Groot et al., 2015; Bedia et al., 2018) or fire activity under projected climate change (Abatzoglou et al., 2018; Jain et al., 2020; Ranasinghe et al., 2021).

Here, we present a new dataset of the FWI, based on climate data from the 6th phase of the Coupled Model Intercomparison Project (CMIP6) and using an improved algorithm. We build upon the work of Abatzoglou et al. (2019) for the previous generation of CMIP models. The novelty of this work comes from (1) the expanded regional applicability thanks to improvements in the original algorithm, (2) using the latest CMIP data covering historical and shared socioeconomic pathways (SSPs), from 1850 to 2100, and (3) providing the whole database to the users, thus enabling a large range of usages. Several packages have proposed different adjustments to the initial algorithm of the FWI. By gathering these improvements, our new algorithm allows us to compare the sensitivity of the product to these modifications. We produce an updated FWI dataset which enables analyses over longer timescales while considering climate sensitivity and internal variability. We envision this open-access dataset of fire weather as a valuable resource for scientists in the fields

of climate change and risk assessment, insurance companies, and forestry agencies.

2 Data and methods

2.1 Climate model data

We use all available CMIP6 simulations (Eyring et al., 2016) of climate models to create FWI data over 1850–2100 using the experiment *historical* and all SSPs (O'Neill et al., 2016; Tebaldi et al., 2021), namely, *ssp119*, *ssp126*, *ssp434*, *ssp534-over*, *ssp245*, *ssp460*, *ssp370*, and *ssp585*. Using all SSP experiments allows us to represent high/low mitigation and adaptation challenges resulting in different radiative forcings by the end of 2100. We retrieve daily maximum temperature (*tasmax*), precipitation (*pr*), wind (*sfcWind*), and minimum relative humidity (*hursmin*) data from all available ensemble members of all available ESMs. More precisely, the FWI is calculated only if the four variables are provided for the experiment. For scenarios, there is an additional condition: it depends not only on the availability for the experiment, but also on whether the corresponding *historical* could be run. The algorithm of the FWI requires the last values of *historical* as initialization for the scenario for continuity reasons (more details are provided in Sect. 2.2). The full list of runs calculated is represented in Fig. 1.

The algorithm for the FWI requires daily temperature, relative humidity and wind speed at noon, and the daily accumulated precipitation (Van Wagner, 1987). Using variables at subdaily resolution would significantly reduce the number of available runs. Instead of noon variables, daily maximum temperature and daily minimum relative humidity can be used, as done for CMIP5 for one ensemble member per model (Abatzoglou et al., 2019).

Some applications may need to maximize the number of ensemble members per model, and thus a second dataset is provided. The first dataset deduces the FWI from daily minimum relative humidity, while the second one uses daily mean relative humidity (*hurs*) instead, because this variable is provided for more model runs. In Sect. 3.4, we provide a sensitivity analysis comparing the FWI based on daily average relative humidity against daily minimum relative humidity, while Fig. A1 summarizes the available runs with daily average relative humidity.

We highlight that using CMIP6 data comes with limitations. Although this is the result of a large community effort (Tebaldi et al., 2021), there may be some biases and discrepancies in these inputs (Wilcox and Donner, 2007; Rossow et al., 2013; Pfahl et al., 2017; McKitrick and Christy, 2020). Analysis of these biases has been performed for temperatures in Fan et al. (2020), regional precipitations (Rivera and Arnould, 2020; Agel and Barlow, 2020; Ajibola et al., 2020), relative humidity (Douville et al., 2022), and wind (Shen et al., 2022). A bias-corrected version of CMIP6 data may be used as inputs, but existing datasets do not provide the necessary variables for the computation of the FWI (Carvalho et al., 2021; Xu et al., 2021), nor the full ensemble that we use here.

2.2 FWI and adjustments

The FWI system consists of several indices calculated in three steps (Van Wagner, 1987; Lawson and Armitage, 2008) as illustrated in Fig. 2. The moisture contents of organic materials are calculated first through the Fine Fuel Moisture Code (FFMC), the Duff Moisture Code (DMC), and the Drought Code (DC). The FFMC rates the moisture content of fine fuels and the litter, hence the probability of ignition. The DMC rates the moisture content of slightly compacted organic layers at medium depth, giving a sense of the fuel consumption. The DC rates the moisture content of deep and compact organic layers, depicting the behavior of slow-burning materials and representing seasonal effects. These three indexes are actually bookkeeping systems, accounting for changes in moisture through precipitation and drying. It is crucial to note that they are unitless and that they are defined "with values rising as moisture content decreases for the best psychological effect" (Van Wagner, 1987), as illustrated with Eq. (5) of Lawson and Armitage (2008).

Afterwards, two indices are deduced from these moisture contents. The Initial Spread Index (ISI) is an indicator of the likely rate of fire spread, while the Buildup Index (BUI) encompasses the fuel available for combustion. Together, they are used to deduce the FWI rating of the fire intensity. It is important to note that the FWI is entirely based on atmospheric variables, only providing a sense of how likely or intense a fire would be under these conditions. Information regarding vegetation is essential for assessing variables such as burned area or fire emissions.

The first published algorithm for the FWI was provided by Simard (1970) and then continuously updated for different programming languages (Wang et al., 2015). The latter source corresponds to the same equations and parameters, and it is hereafter referred to as the original algorithm. It has been translated into several packages, although with several adjustments, expanding the initial focus on Canadian forests for an adaptability to other regions. These adjustments make use of or extend further the suggestions from Lawson and Armitage (2008). In this current study, we implement in python the major options for the three types of adjustment described below (day length, "drying factor", and overwintering) and test their effect applied to all latitudes and to bins of latitude in Sect. 3.1 to 3.3. To our knowledge, the effects of such adjustments have not been published, except for overwintering (McElhinny et al., 2020). The details of the considered packages are provided in Table 1.

During the calculation of the DMC, the effective day length is used, and several packages proposed alternatives to day lengths adapted to Canada and the month of the year. A

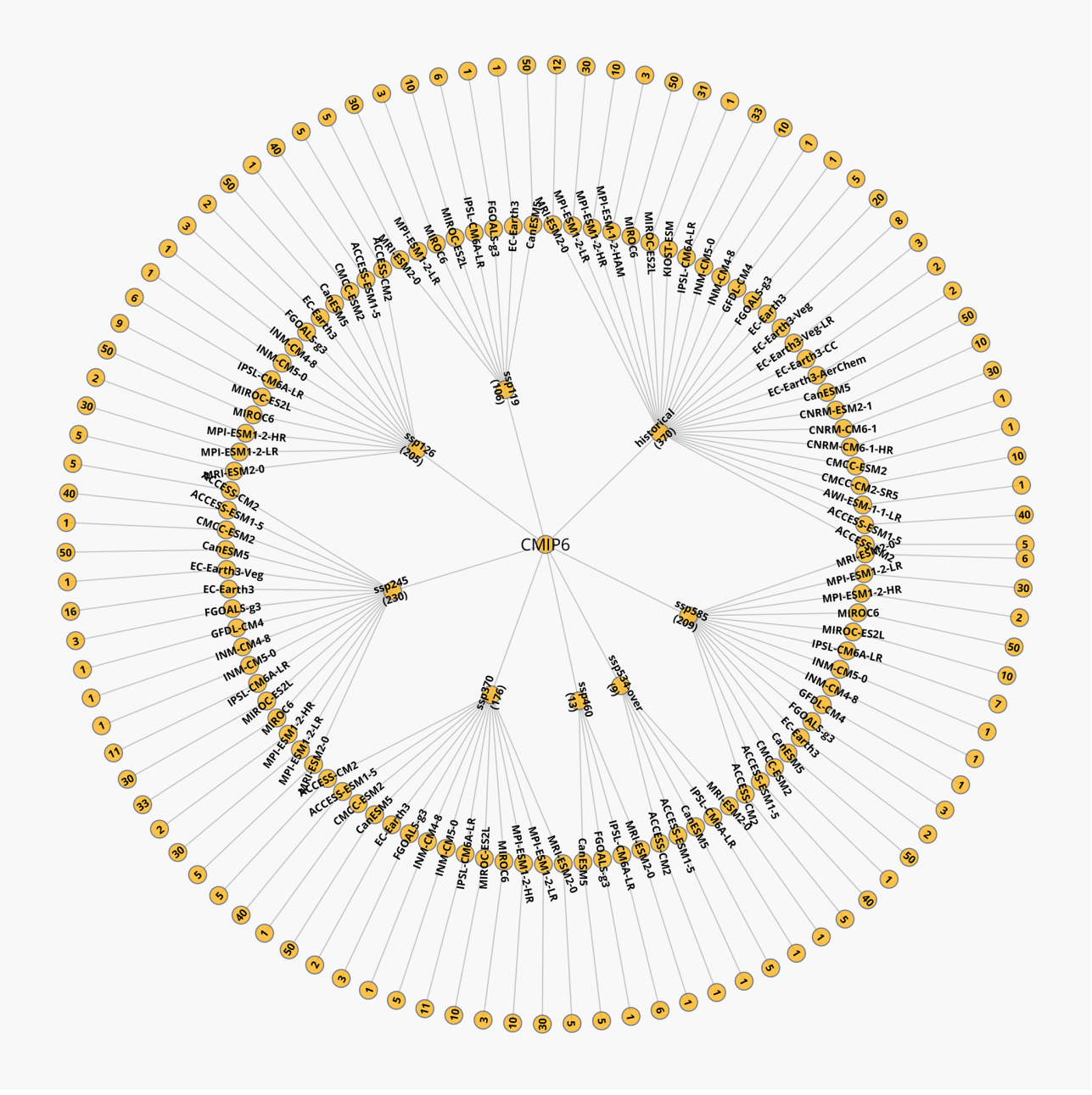

Figure 1. Runs used throughout the study. For each experiment, each ESM is selected if at least one ensemble member is available and valid for all the variables used as input for the calculation of the FWI. The outermost circle indicates the corresponding number of ensemble members of each ESM and scenario. Altogether, 1321 runs are used here.

longer effective day length would reduce the moisture content of slightly compacted organic layers.

During the calculation of the DC, a parameter called "day-length adjustment" is used to calculate the potential evapotranspiration, i.e., as a drying factor of the compact organic layers. Several packages propose adapting this value depending on the hemisphere. To avoid confusion with the adjustment brought to effective day length, we call this parameter the drying factor.

Besides adjusting for the drying factor, Lawson and Armitage (2008) give details on how to overwinter the DC component to account for the effects of abnormally dry winters. The effects of dry or wet winters would not carry over up to spring in the fine fuels (FFMC) or in the moderately compacted organic layers (DMC) but may for the compact organic layers (DC). In the original algorithm (Wang et al., 2015), the moisture content of deep organic layers is almost saturated in spring, even though this should not be the case

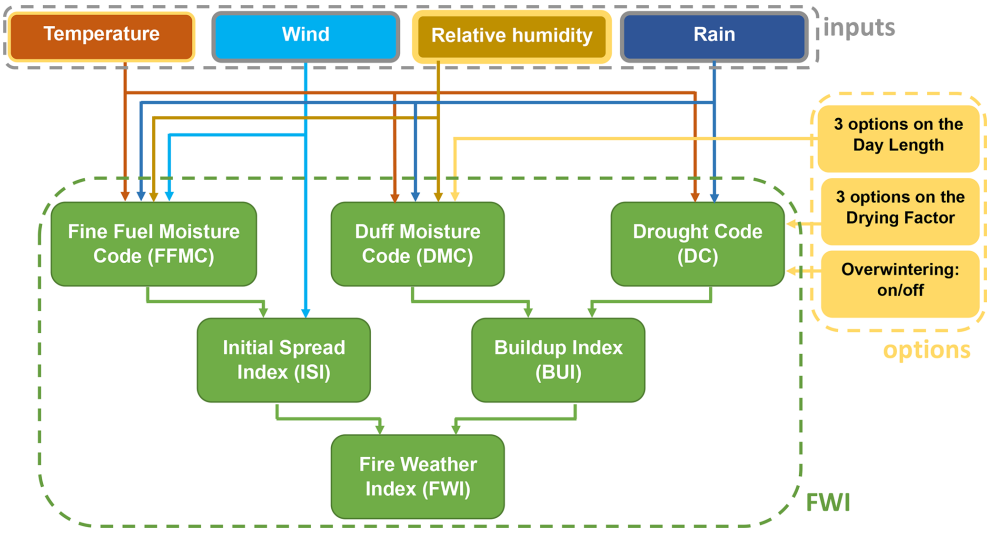

Figure 2. Conceptual structure for the calculation of the Fire Weather Index (inspired by the figure at Natural Resources Canada, 2022). The drying factor is an adjustment to the day length used for drying in the Drought Code (DC), renamed here to avoid confusion with the effective day length.

Table 1. Details of the adjustments for each one of the codes considered. The codes for each package are available online (Wang et al., 2015; pyfwi, 2022; NCAR/fire-indices, 2022; cffdrs, 2022). The drying factor is an adjustment to the day length used for drying in DC, renamed here to avoid confusion with the effective day length. Options in bold are those used for the data provided by this study.

Adjustment	Method		Package				
	Name	Description	Original	pyfwi	NCAR	cffdrs	Current study
Effective day length (DMC)	Original	Values depending on the month	**X**				**X**
	Bins of lat.	Bands of latitude (° N): [−90, −30]; [−30, 0]; [0, 30]; [30, 90]		**X**			**X**
		Bands of latitude (° N): [−90, −30]; [−30, −10]; [−10, 10]; [10, 30]; [30, 90]				**X**	
	Continuous lat.	Function of latitude of grid cell and day of year			**X**		**X**
Drying factor (DC)	Original	Values depending on the month	**X**		**X**		**X**
	Two hemispheres	Depends too on the hemisphere: Northern identical and Southern shifted by 6 months		**X**			**X**
	Two hemispheres and tropics	Bands of latitude (° N): identical for [20, 90], shift of 6 months for [−90, −20], average for [−20, 20]				**X**	**X**
Overwintering (DC)	Original	No	**X**				**X**
	Overwintering	Yes				**X**	**X**

in regions with dry winters. The adjustment for overwintering uses the value of DC at the end of the fire season and the precipitation up to the start of the fire season, as defined in McElhinny et al. (2020). The onset of the fire season is defined here when the temperature is above 12 °C for the current day and the next 2 d and up to when the temperature is below 5 °C for the current day and the 2 former days (Wotton and Flannigan, 1993). We note that two parameters are introduced by the overwintering adjustment, which are the carry-over fraction of last fall's moisture and the effectiveness of winter precipitation in recharging moisture reserves in spring. The value of the carry-over fraction depends mostly on the local snow cover, and a bare soil during winter has a fraction of 0.5, while a thick cover would increase

it to 1. Because we do not have this information from the ESMs, we use 0.75 as a default value everywhere. The second parameter, the effectiveness of winter precipitation, depends mostly on the soil type: well-drained soils would favor percolation and runoff and thus a low fraction of 0.5, while poorly drained soils would be more efficient with a fraction of 0.9. Similarly, without this information from the ESMs, we use 0.75 as a default value everywhere. This adjustment is initially developed for northern latitudes (Van Wagner, 1987), hence the terms of fall, winter, and spring, but it is applied here for all the latitudes.

The three moisture codes keep track of the past climate, changing every day the values of DMC, DC, and FFMC with the current weather and the values on the former day. This implies that the scenarios are initialized with their corresponding historical run, the same ESMs, and the same ensemble members. The full time series are used for calculation of the FWI, without any interruption out of the fire season, to conserve the full continuity. For the historical period, the values are initialized using the proposed method in Lawson and Armitage (2008).

2.3 Database features

After calculation of the FWI on the native grid of the ESM, we then use second-order conservative remapping (Jones, 1999; Brunner et al., 2020) to regrid them onto a common $2.5° \times 2.5°$ longitude–latitude grid to enable comparison across different models.

Annual indicators are made available and presented in Sect. 3 to illustrate these data and ease their interpretation. We use the four following annual indicators, all of them defined in Abatzoglou et al. (2019) and Jolly et al. (2015), although with a reference period of 1850–1900 instead of 1861–1910.

- An extreme value of the FWI (*fwixx*): local annual maximum value of the FWI
- Number of days with extreme fire weather (*fwixd*): local annual number of days above the local threshold defined as the 95th percentile of the FWI over the reference period
- Length of the fire season (*fwils*): local number of days above the local threshold defined as the mid range of the extrema in the FWI over the reference period.
- Seasonal average of the FWI (*fwisa*): local annual maximum of the 90 d running average of the FWI.

Here, *fwixd* uses a definition of what "extreme" fire weather is based on the 95th percentile like in Abatzoglou et al. (2019) and not an absolute set of classes. This approach generalizes the method for analyzing the FWI, which attributes fire danger classes (e.g., "very low", "low", "moderate", "high") to intervals of values. These classes are rather used for local or regional cases and are hence defined for the region, such as China (Tian et al., 2011), Europe (San-Miguel-Ayanz et al., 2022), Greece (Varela et al., 2018), Ontario (Martell, 2000), and Malaysia and Indonesia (Dymond et al., 2005; de Groot et al., 2007). The proposed procedure to define these classes is to assume how many extreme days should be allowed on average for each season and todeduce the threshold for the "extreme" class from this assumption and a sample of the FWI over a reference period. In our case, we cover the whole Earth, and the "extreme" fire danger class needs a consistent definition. By assuming a local threshold based on the 95th percentile, it is consistent with the assumption of about 18 d per year that is considered locally as extreme fire weather. No other fire danger classes are used by our other annual indicators.

As a remark, there are two definitions for the fire season, which are kept for consistency reasons. The adjustment for overwintering DC uses a definition of the fire season based on temperature thresholds as described in Wotton and Flannigan (1993). However, according to Abatzoglou et al. (2019), the annual indicator *fwils* defines the fire season when the daily FWI is above a local threshold defined as the average of the minimum and the maximum of the FWI in the reference period.

Given that the FWI is calculated only using atmospheric variables, regardless of the vegetation cover, we mask the results according to the ESA CCI land cover of 2016 (ESA-CCI, 2017, 2019). Similarly to Abatzoglou et al. (2019), when more than 80 % of the surface of the grid cell is flagged as bare areas, water, snow, and ice or sparsely vegetated, it is considered to be infrequent burning.

No bias correction is applied here, as it is not within the scope of this paper and because the method may depend on the intended application of the FWI. One may decide to correct the FWI through adjustments in the four inputs of the algorithm via various possible ways to account for climate model biases (François et al., 2020), while others may prefer to correct the FWI itself through observation-based FWI (Field et al., 2015; Field, 2020).

3 Results

3.1 Sensitivity to the adjustments on the day length

As indicated in Table 1, several adjustments are introduced to the effective day length used for the calculation of the DMC. We show the effect of these adjustments in Fig. 3 with example maps for 1 July 2014 and climatologies. Figure A2 replicates Fig. 3, albeit for 1 January 2014. The DC and FFMC are not represented, because they are not affected by this factor. The adjustments mostly change values in the Southern Hemisphere, where the effective day lengths were not prepared in the original calibration. For instance, in December–January, when the fire season is active in southern land, a longer effective day length means a slightly drier organic layer. As

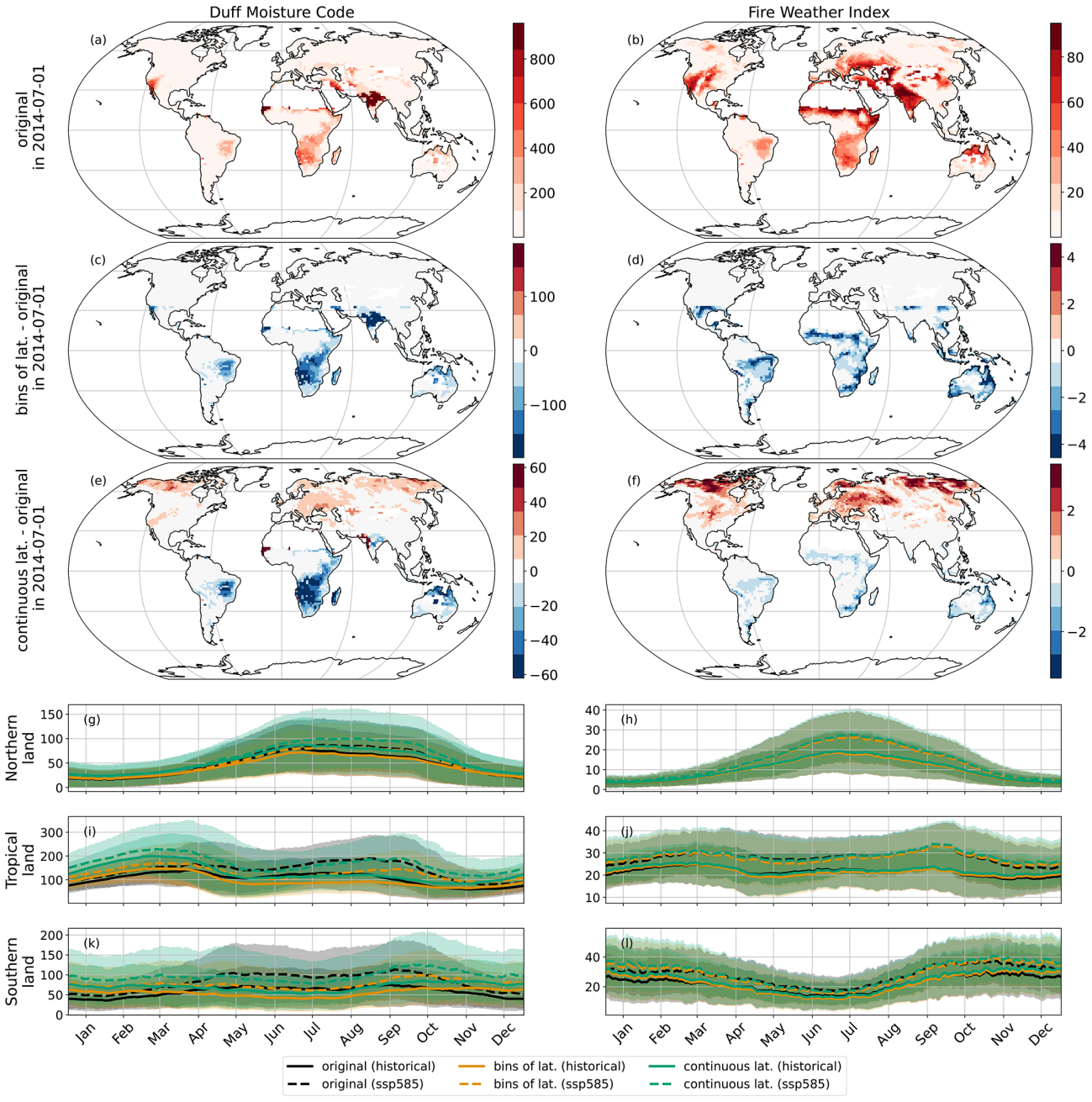

Figure 3. Sensitivity to the day length factor of the ESM ACCESS-CM2 in the experiments *historical* and *ssp585* over the ensemble member r1i1p1f1. The first row of maps **(a, b)** shows the values of the DMC and the FWI, the first and final indices affected by this factor, in the original version of the algorithm (Wang et al., 2015). The following maps (**c**–**f**) show the differences with the adjusted version of the algorithm (Table 1). The following rows show the daily climatologies over 1995–2014 (solid line) and 2081–2100 (dashed line), represented in terms of the average and ± 1 standard deviation ranges. Northern land **(g, h)** is defined as grid cells over 20° N and is not marked as infrequent burning. Similarly, southern land **(i, j)** is below 20° S, and tropical land **(k, l)** is the intermediate latitude band.

moisture content decreases, the DMC values increase, and so does the FWI. We note that using the day length function (daylight_fao56, 2022) tends to extend the day length, thus increasing the FWI in northern land as well.

For the first adjusted version (pyfwi, 2022), the day is shorter below 30° N, and thus the drying is lower (Fig. 3c–f). In southern land, this version increases the DMC by up to 62 % in December–January and decreases the DMC by −38 % in June–July (Fig. 3k). In 2081–2100 of *ssp585*,

these differences change, respectively, to 60 % and −36 %, and then with just a slight reduction of the range (Fig. 3k). This reduction might be due to the stronger drying regime at the end of *ssp585* compared to the historical period, causing this adjustment affecting drying not to matter as much. With a lower DMC, the BUI is reduced, thus decreasing the FWI (Fig. 3l). The FWI is then increased by up to 14 % in December–January and decreased by up to −14 % in June–July. The range of the change in the FWI changes to 15 % and −10 % in 2081–2100 of *ssp585*. Tropical and northern land are less affected because the magnitude of the adjustment to the effective day length is smaller (Fig. 3g–j).

For the second adjusted version (NCAR/fire-indices, 2022) in southern land, the FWI is increased by up to 19 % in December–January and decreased by up to −6 % in June–July (Fig. 3k–l). In 2081–2100 of *ssp585*, the range of these differences is changed to 21 % to −5 %. However, northern land is also affected, with an increase in the FWI by up to 10 % in December and only by 1 % in April.

3.2 Sensitivity to the adjustments in the "drying factor"

The drying factor has also received several adjustments in the considered packages (Table 1 and Fig. 4). We note that the original name of this factor is "Day-length adjustment in DC" (Wang et al., 2015), but it is renamed here to avoid confusion with the adjustments brought to the "effective day length". Figure 4 shows the effect of the adjustments brought to this drying factor through maps on 1 July 2014 and climatologies, while Fig. A3 shows its equivalent on 1 January 2014. The DMC and FFMC are not represented here, because they are not affected by this factor.

As described in Table 1, the original code proposes a single monthly value over the Earth, while the first adjustment (pyfwi, 2022) proposes one monthly value for each hemisphere, and the last one (NCAR) goes further by adding one constant value between 20° S and 20° N. In Fig. 4, this is why this adjustment has mostly an impact below 20° S and to a lesser degree between 20° S and 20° N. For this reason, and similarly to Fig. 3, we mainly discuss here the effect in southern land, which is identical in the two adjusted versions. For 1 July 2014, DC is lower in the adjusted versions (Fig. 4). According to the algorithm, the drying factor is lower in July at these latitudes, causing a lower potential evapotranspiration, consistent with a higher moisture content and a lower DC.

The major differences for the DC in southern land, below 20° S, are an increase by up to 43 % in February–March and a decrease by up to −38 % in July–September. The adjustment to the drying factor in southern land is at its peak in July and at its minimum in January, 1 month before the observed maxima in the differences in DC. With a lower DC, the BUI is also decreased, causing the FWI to decrease. In southern land, the FWI increases by up to 4 % in February–March and decreases by up to −4 % in July–September.

This adjustment has a smaller impact on FWI than on DC and is also relatively lower compared to the effect of the adjustment on the effective day length. However, sensitivities of FWI are by increasing order to FFMC and then DMC and finally DC (Dowdy et al., 2010), mostly because a fire starts with the least compact organic layers to move to the most compact ones. Even though this adjustment has a relatively low impact, for latitudes below 20° S, these adjustments help in adapting the climate effects on the most compact organic layers, which is of interest to reproduce seasonal cycles and long-term effects of climate change (Van Wagner, 1987).

3.3 Sensitivity analysis to the overwintering

Overwintering the DC was suggested in Lawson and Armitage (2008) to account for the effects of abnormally dry winters as explained in Sect. 2.2. This adjustment affects mostly the DC above 20° N because of the climatological conditions at these latitudes. The stronger impact can be seen during northern winter. Figure 5 illustrates the effect of this adjustment for 1 July 2014 and climatologies, while Fig. A4 does so for 1 January 2014. As expected, this adjustment affects mostly the DC above 20° N and the winters below 20° N are not dry enough, except in the south of Argentina and Chile.

We observe a reduction in DC by up to −55 % in December–January in northern land. The DC is decreased over the full year, the minimum of this reduction being −6 % in July–September. By definition, a lower DC means a higher moisture content of compact organic layers. Normally, the moisture content after a dry winter should be lower than after an average winter. In the default algorithm, the calculation of the FWI stops during winter and resumes in spring. To initialize the calculation in spring, DC uses the default value of 15 as a saturated moisture content (Van Wagner 1987). This leads to an overestimation of the moisture content in spring, especially after dry winters. Similarly to Abatzoglou et al. (2019), in the version called "original", we run the full time series, without interruption in winter, meaning no initiation of the DC with a saturated level. In Fig. 5, we see that adding overwintering increases the moisture content in winter and spring. This implies that running the full time series with the default code tends to overestimate the drying during winter. In this sense, this is consistent with McElhinny et al. (2020). The added value of overwintering is to balance the overestimation of spring moisture content when interrupting calculation of the FWI or the underestimation of spring moisture content in uninterrupted calculation of the FWI.

With too dry moisture content in the compact organic layers, the FWI in northern land tends to be higher in the original version (which runs the code throughout the year) relative to the overwintered version. Overwintering reduces the FWI by up to −18 % during January–February and brings an important adjustment to DC. Calculating the full time series of FWI means not reusing the saturated starting value for spring

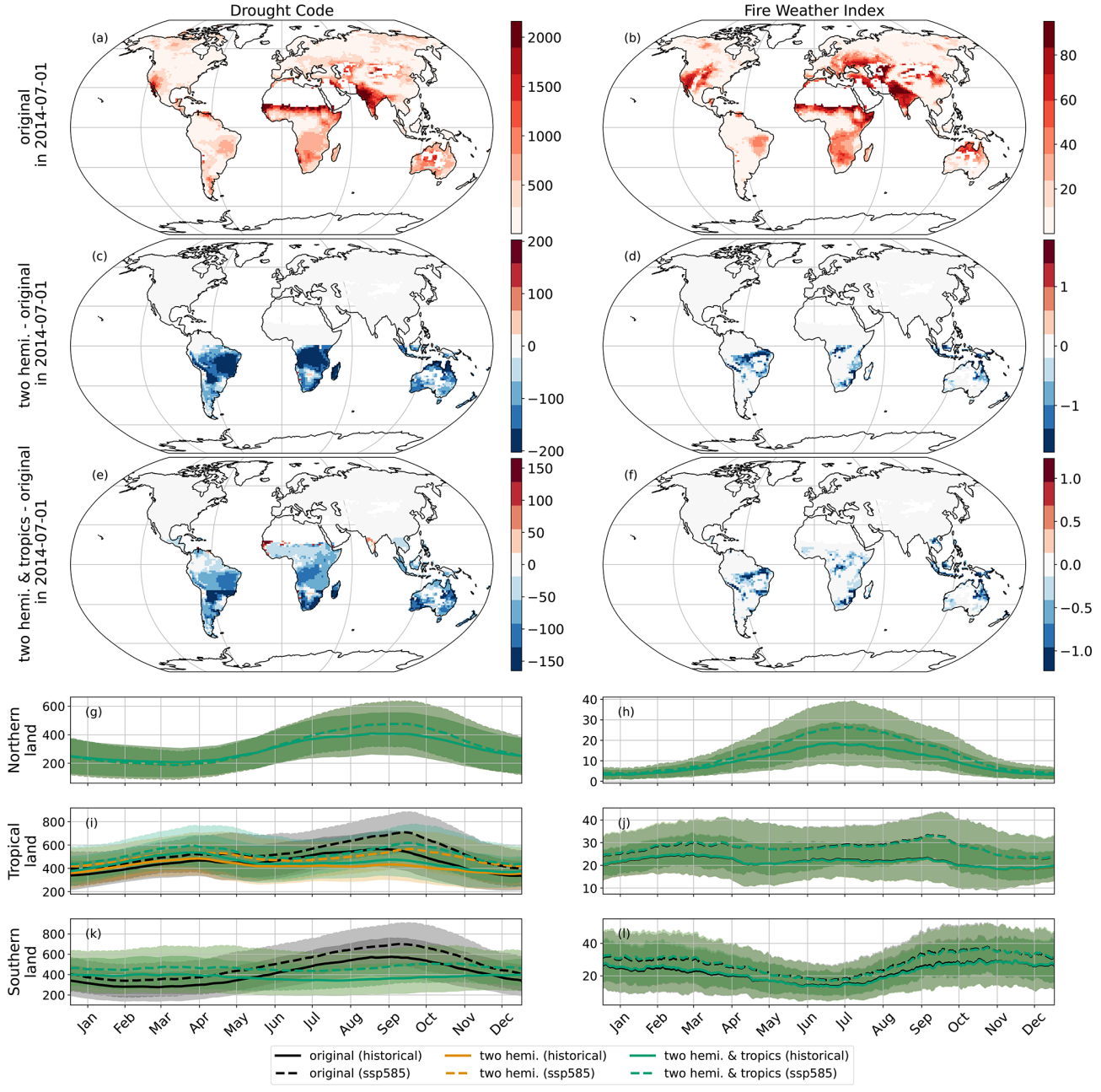

Figure 4. Sensitivity to the drying factor of ACCESS-CM2 in the experiments *historical* and *ssp585* over the ensemble member r1i1p1f1. The first row of maps **(a, b)** shows the values of the DC and the FWI, the first and final indices affected by this factor, in the original version of the algorithm (Wang et al., 2015). The following maps (**c** to **f**) show the differences with the adjusted version of the algorithm (Table 1). The following rows show the daily climatologies over 1995–2014 (solid line) and 2081–2100 (dashed line), represented in terms of the average and the ± 1 standard deviation range. Northern land **(g, h)** is defined as grid cells over 20° N and is not marked as infrequent burning. Similarly, southern land **(i, j)** is below 20° S, and tropical land **(k, l)** is the intermediate latitude band.

DC, causing moisture content over the year to be too low, and hence the DC is too high. We consider that overwintering is necessary when adjusting this effect in full time series.

3.4 Sensitivity to using daily mean relative humidity

The default approach would be to use as inputs daily minimum relative humidity and daily maximum temperature. As explained in Sect. 2.1, here we use daily mean relative humidity as an alternative, because daily minimum relative hu-

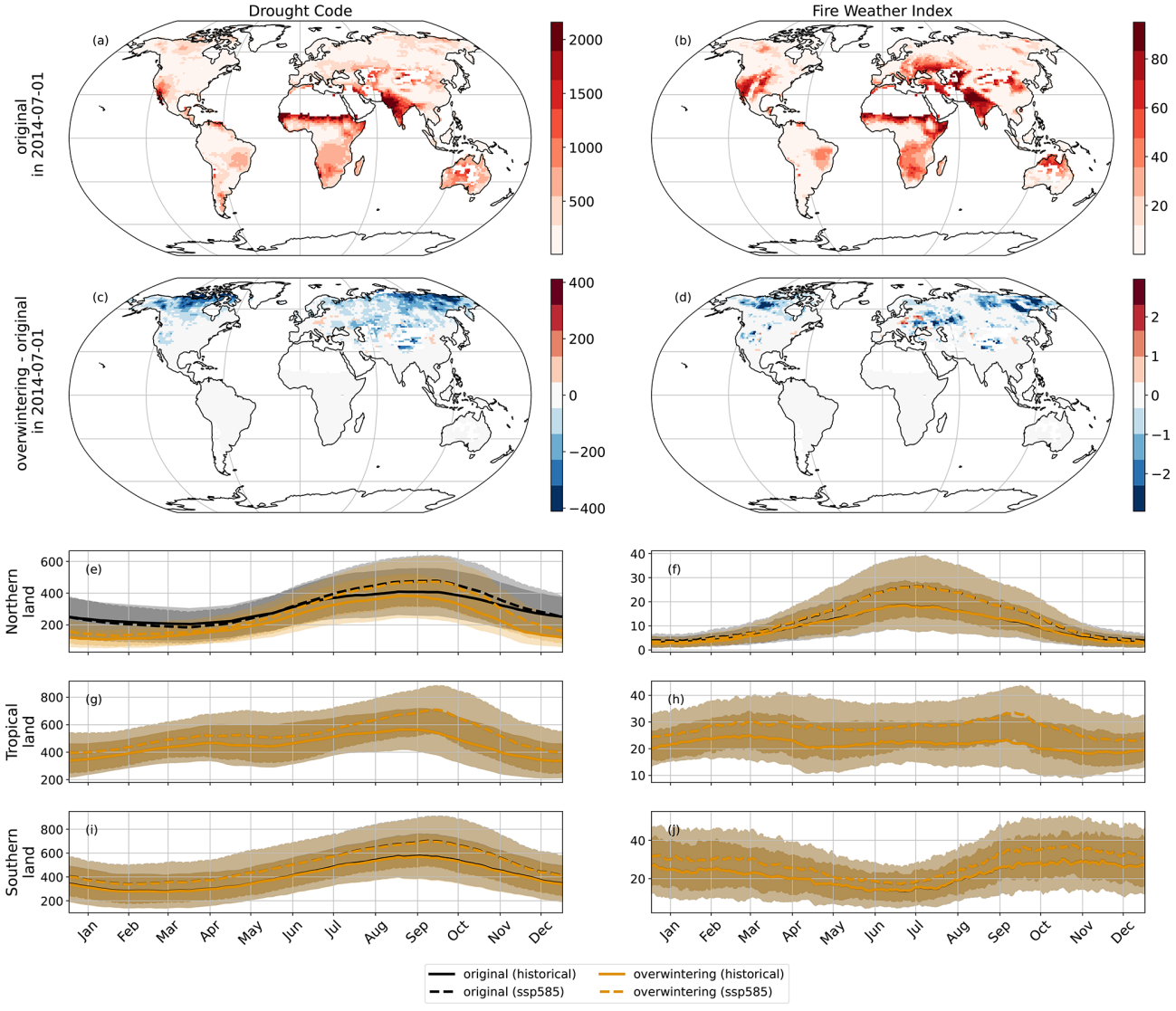

Figure 5. Sensitivity to the overwintering of ACCESS-CM2 in the experiments *historical* and *ssp585* over the ensemble member r1i1p1f1. The first row of maps **(a, b)** shows the values of the DC and the FWI, the first and final indices affected by this factor, in the original version of the algorithm (Wang et al., 2015). The following maps **(c, d)** show the differences with the adjusted version of the algorithm (Table 1). The following rows show the daily climatologies over 1995–2014 and 2081–2100, represented in terms of the average and ± 1 standard deviation range. Northern land **(e, f)** is defined as grid cells over 20° N and is not marked as infrequent burning. Similarly, southern land **(g, h)** is below 20° S, and tropical land **(i, j)** is the intermediate latitude band.

midity is not provided for many CMIP6 runs, reducing the total number of runs from 1486 to 1321. We show in Fig. 6 the influence of this choice, with climatologies and maps for 1 July 2014. Figure A5 extends this figure using the maps for 1 January 2014.

The DC takes as climate inputs only temperature and precipitation but not relative humidity. This component is therefore not affected by this choice. Using daily mean relative humidity instead of the daily minimum relative humidity increases the moisture content of the other two components, as evidenced by lower DMC and FFMC. For DMC, it is reduced above 20° N by −25 % (January) to −21 % (October–November). In tropical land, between 20° N and 20° S, this reduction changes to −15 % (March–April) to −28 % (June–July). Finally, below 20° S, the DMC is reduced by −34 % (June–July) to −20 % (November–December). The reductions tend to be stronger for FFMC, ranging from −45 % in June below 20° N to −22.7 % between 20° S and 20° N. With a more humid climate as input and consequent lower DMC and FFMC, the FWI itself is reduced. During the fire season, the FWI is reduced by about −33 % (June) above 20° N, −35 % between 20° S and 20° N (May), and −29 % (December) below 20° S. Over 2081–2100 of *ssp585*, these reductions of the FWI are changed to −31 % (June) above

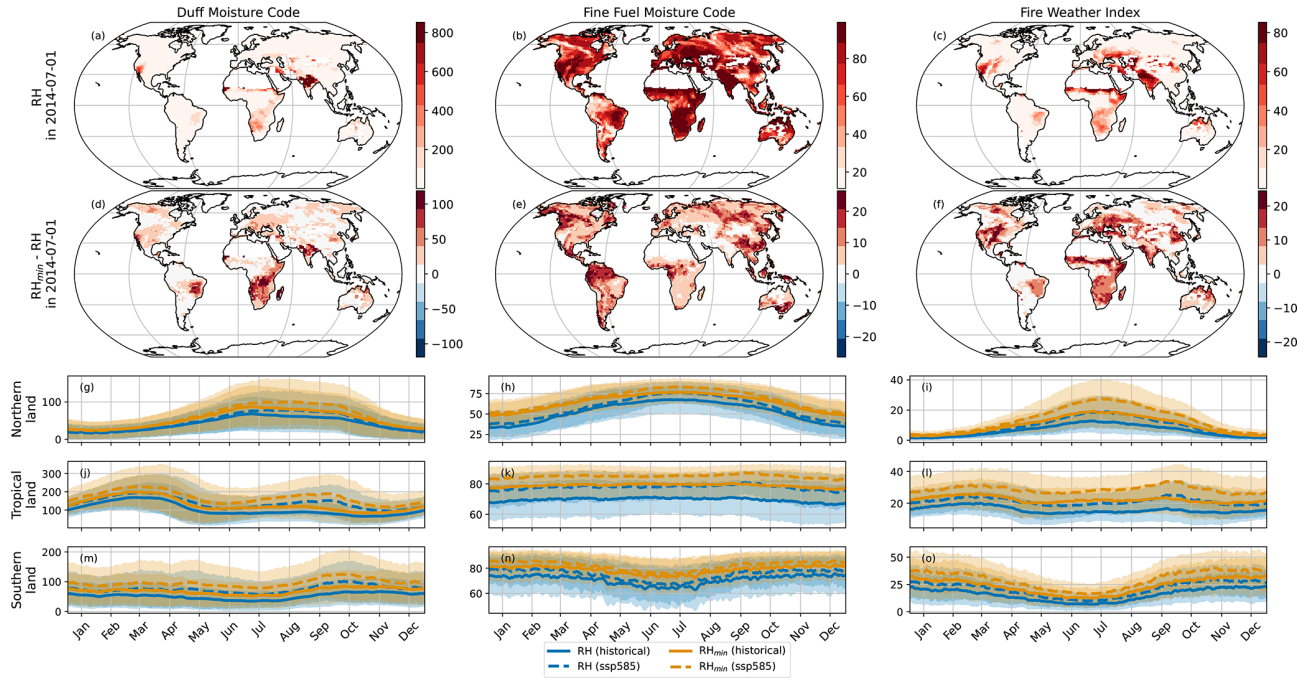

Figure 6. Sensitivity to the variable used for daily relative humidity of ACCESS-CM2 in the experiments *historical* and *ssp585* over the ensemble member r1i1p1f1. The first row of maps (**a** to **c**) shows the values of the DMC, the FFMC, and the FWI, the first and final indices affected when run with daily average relative humidity. The following maps (**d** to **f**) show the differences when run with daily minimum relative humidity. The following rows show the daily climatologies over 1995–2014 and 2081–2100, represented in terms of the average and ± 1 standard deviation range. Northern land (**g** to **i**) is defined as grid cells over 20° N and is not marked as infrequent burning. Similarly, southern land (**j** to **l**) is below 20° S, and tropical land (**m** to **o**) is the intermediate latitude band.

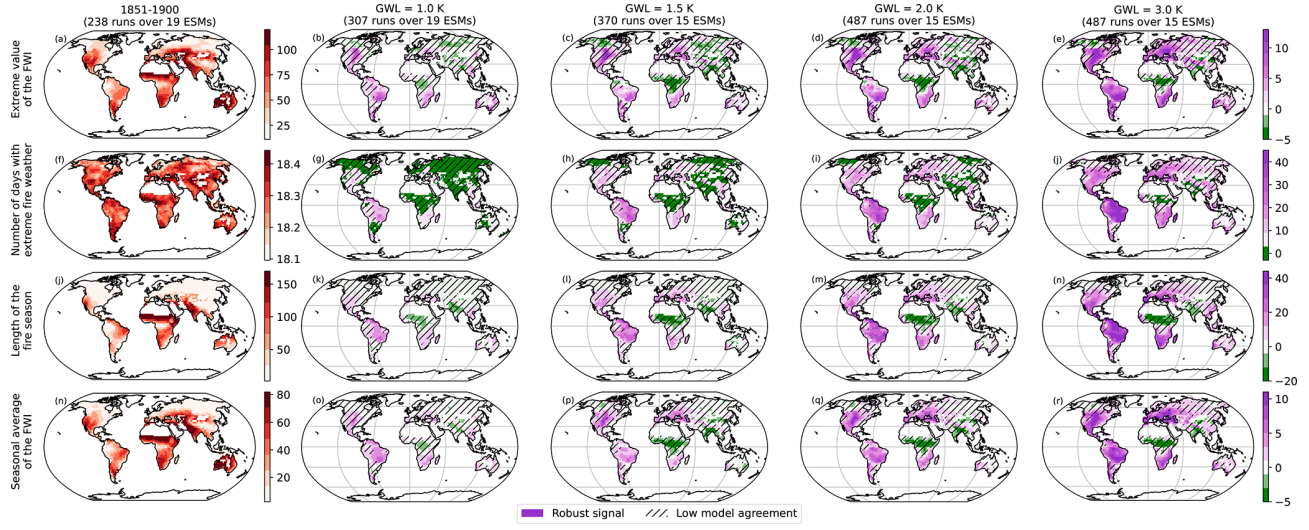

Figure 7. Averages of annual indicators at the preindustrial and changes in averages at different global warming levels (GWLs). The average maps in 1851–1900 are shown in panels **a**, **f**, **j**, and **n** for the four annual indicators. Each column corresponds to the changes in averages at different GWLs, each row corresponding to a different annual indicator. The agreement of models in the sign of the change is used to define the robustness of the signal. More details are provided in Text A1.

20° N, −30 % (June) between 20° S and 20° N and −25 % (November) below 20° S.

We note that the reduction in the FWI caused by using mean relative humidity instead of minimum relative humidity is roughly identical during the fire seasons across the planet, be it over 1994–2014 or 2081–2100. This implies that analysis based on relative changes in the FWI would not be strongly affected by this choice. As discussed in Sect. 2.1, the annual indicators are provided for both cases, i.e., using daily mean relative humidity and using daily minimum relative humidity.

3.5 Main results

As illustrated in Fig. 1, the FWI was calculated for a total of 1321 runs, deduced from 28 ESMs, run over the historical period (1850–2014) and over eight scenarios (2015–2100) and with a total of 108 different ensemble members. To synthesize these gridded daily products, annual indicators are provided, as detailed in Sect. 2.3. To summarize these annual indicators, we choose to show their evolutions at different global warming levels (GWLs) in Figs. 7 and 8 while representing the robustness of the signal. Figure 7 shows the average of the runs at each GWL, and Fig. 8 shows the 90th percentile. A signal is defined as robust where at least 80 % of the models agree on the sign of the change with reference to 1851–1900. More details on the method used to synthesize these data are provided in Text A1 of the Appendix.

In Fig. 7, we observe that all robust signals in the annual indicators of the FWI show an increase. In other words, there is nowhere on Earth where ESMs agree at 80 % or more on a decrease in fire weather, in any of the four annual indicators represented here. For most regions of Earth and incremental warming levels, all four annual indicators show an increase in their average, even if this signal is not robust in all regions. Still, there are non-robust decreasing trends in the average in central Africa, India, and north of the Tibetan Plateau. This concerns the length of the fire season, the annual maxima, and the seasonal average of the FWI but not the number of days with extreme fire weather that continue to show an increasing trend in these regions. The regions with robust signals are central North America, northern South America, Europe, southern Africa, and Australia. We note the higher GWL and the larger spatial extent of the robustness of the signal across the regions.

From Fig. 7, we infer that the annual maximum of the FWI has increased by up to +37 % with a GWL of 1.0 °C. With a GWL of 3.0 °C, this indicator is increased by up to +120 %, its average being +9 %. Western Australia exhibits the highest robust trend for this indicator. The number of days with extreme fire weather has increased by up to +128 % with a GWL of 1.0 °C. With a GWL of 3.0 °C, it increases by up to a factor of 5.0, while its average is +86 %. South America would be the most affected with 48 d of extreme fire weather per year, while the world would have on average 26 d. The length of the fire season increases as well, even at a GWL of 1.0 °C, up to a factor of 4.0. With a GWL of 3.0 °C, it may increase by a factor of 15.0 and on average +66 %. Such a high relative increase happens in northern Siberia, where the statistical distribution of the daily FWI and the definition of this indicator lead to an extremely short fire season. Nevertheless, the average increase by +66 % shows that the fire season is overall increasing, lasting about 45 d on average. At a GWL of 1.0 °C, the seasonal average of the FWI is also increasing, by up to 56 %. However, at a GWL of 3.0 °C, it increases by up to +250 % and on average by +17 %. Indonesia would be the most affected region according to this criterion.

Overall, these annual indicators emphasize that, under climate change, atmospheric conditions tend to increase the number and intensity of fires. An approximate estimate is that we would expect at least an average +66 % in both the frequency and the duration of fires at a GWL of 3.0 °C relative to 1851–1900, although this is highly dependent on the metric and the region.

In analogous fashion to Fig. 7, we show the FWI indicators of the 90th percentile in Fig. 8. The 20-year window centred at the time of exceedance of the GWL is used here to deduce the 90th percentile instead of the average. It assumes that, over the 20 years at each GWL, the distributions of the annual statistics of the FWI are stationary enough such that the contribution of the local warming trend is lower than the local natural variability. Under this assumption, the percentiles of all runs exceeding the GWL provide the local 1-in-10-year event and the local model agreement. More details are provided in Text A1 of the Appendix. In Fig. 7, all robust signals are increasing trends, while decreasing trends are always non-robust signals. In Fig. 8, all signals, robust or not, are increasing trends. Regarding the robustness of the signal, we notice that the area extent of the robust signals is higher for the 90 % percentile than for the average. In other words, even if ESMs may disagree in some regions on the sign of the average change in annual indicators of the FWI, they agree much more that 1-in-10-year fires will be higher. As a summary for these trends, at a GWL of 3.0 °C, we calculate an average relative increase in the 1-in-10-year events of +31 % for the annual maximum of the FWI, +192 % for the number of days with extreme fire weather, +177 % for the length of the fire season, and +46 % of the seasonal average. Overall, the 1-in-10-year events would thus almost triple in duration and increase by at least 31 % in strength. These findings highlight how fire management, even more than nowadays, would increasingly become an absolutely crucial element of forest protection across the world. However, there would be some limits to the adaptation possible to these projected changes, highlighting that the best course of action would require limiting global warming to as low as possible.

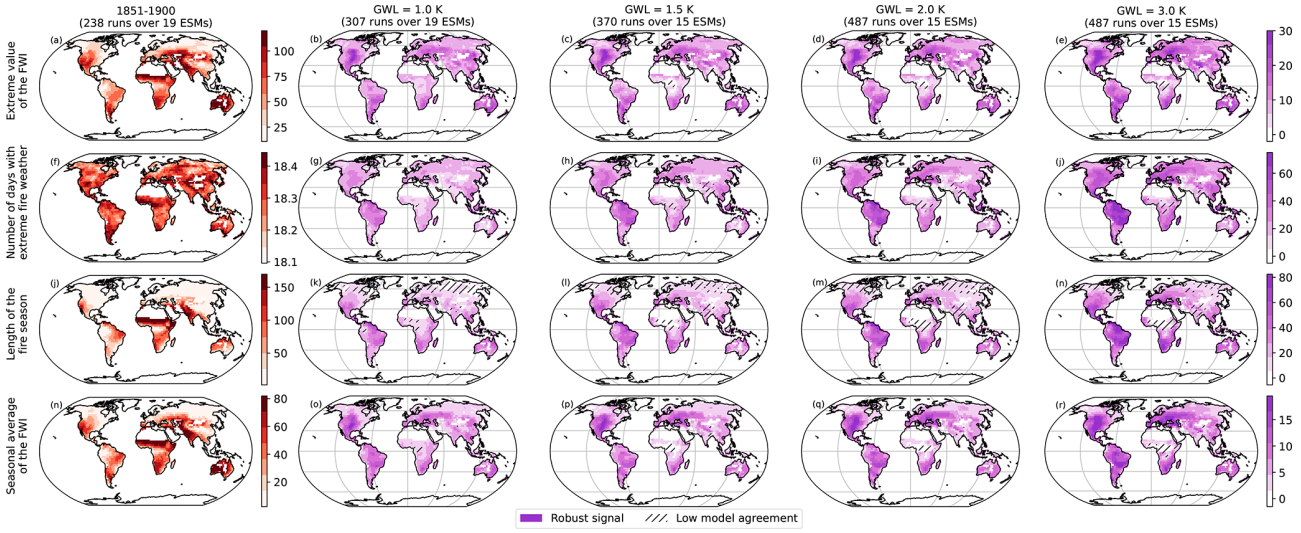

Figure 8. 90th percentiles of annual indicators at preindustrial and changes in averages at different GWLs. The average maps in 1851–1900 are shown in panels **a**, **f**, **j**, and **n**) for the four annual indicators. Each column corresponds to the changes in the 90th percentiles at different GWLs, each row corresponding to a different annual indicator. The agreement of models in the sign of the change is used to define the robustness of the signal. More details are provided in Text A1.

4 Data availability

The Fire Weather Index data have been generated using data archived in the ETH Zurich CMIP6 repository. CMIP6 model outputs can also be accessed through different Earth System Grid Federation (ESGF) data nodes. The Fire Weather Index produced in this paper is made available in netCDF format, and it is openly and anonymously accessible through https://doi.org/10.3929/ethz-b-000583391 (Quilcaille and Batibeniz, 2022). All files are stored as .zip in the archive. They are named "[Long name of the fire weather indicator] for all available CMIP6 runs (computed using [Long name of the humidity used for calculation])". Each .zip file contains the results for this indicator for different ESMs, scenarios, and ensemble members. For storage reasons, some of them are stored in several parts. Within each of the .zip files, the results for each Fire Weather Index, ESM, scenario, and ensemble member are saved individually in separate files in netCDF4 format under the name "[indicator]_ann_[ESM]_[scenario]_[member]_g025.nc". Here, "ann" designs the annual resolution, while "g025" designates the name of the grid.

5 Code availability

The Fire Weather Index results have been generated using the open-source model developed by Yann Quilcaille and improved by Yann Quilcaille and Fulden Batibeniz. The code to reproduce the results of this paper is available in a repository on GitHub (https://github.com/yquilcaille/FWI_CMIP6, last access: 26 May 2023 and https://doi.org/10.5281/zenodo.7971275, Quilcaille et al., 2023).

6 Usage notes

The provided data are produced by the Institute of Atmospheric and Climate Science Institute of ETH Zurich. This is an open-source and entirely free dataset. To illustrate possible paths for data users, we indicate in the following list some of the many opportunities where this dataset could be used. Some may rather be considered research questions, while some other points may be of interest for societal issues regarding fires.

As detailed in Sect. 2, we highlight that CMIP6 data may come with biases, while observations provide more realistic inputs and information for fire-related studies. However, observations have lower temporal and spatial availability and cover only the historical period. Thus, model-based data facilitate large-scale analysis.

- Comparison of FWI results with observations to evaluate the biases in the models. Compared to observations, some models show biases in their outputs. How does that affect the calculation of a compound product like the FWI? The FWI can be calculated using data based either on models or on observations (e.g., Vitolo et al., 2019). One may use the dataset provided here to evaluate the discrepancies and eventually how it affects future projections in fire weather. A first work in this direction has been produced with 16 ESMs and one ensemble member over the historical period (Gallo et al., 2022).

- Discrepancies in the FWI across ESM projections. The ESMs show different regional evolutions in some variables, though the effect of these discrepancies on the FWI remains unclear. One may investigate how much projections in fire weather depend on the ESM by using the provided dataset and investigate reasons for the (dis)agreements.

- Dependencies of the FWI on ensemble members. The former path could be extended to the ensemble members. An uncertainty in the projections of the FWI arises from the initial conditions as well. The provided dataset may be used to assess this uncertainty and eventually the natural variability in the FWI.

- Dependencies of the FWI on scenarios. Another dimension of projections in the FWI is the choice of the scenario. Under low warming scenarios, the Earth system gets more time to stabilize, allowing for different regimes, e.g., in the water cycle. This may help to investigate the response of the fire regimes across different scenarios. For example, the differences between low warming or high warming scenarios or even overshoot scenarios can be investigated using the provided dataset.

- This can be used to understand the effects of humidity regimes on fire regimes: minimum relative humidity and average relative humidity have different dynamics, and it is still unclear how they may affect the dynamics of fire weather in current and future climates. The provided dataset may help in assessing these regimes and their differences.

- Comparison of the climatology of the FWI in preindustrial, current, and future climates. Figure 8 of this paper gives a brief overview of this path. What should we expect from fire weather at different levels of climate change? Such a question would be of interest to inform society of the implications of climate change, and the provided dataset may help to answer it.

- Relationship of fire weather with modelled burned area. There is literature showing the correlation between the FWI and burned area (Jones et al., 2022), in spite of other relevant factors such as fire ignition. One may use the provided dataset to check in the CMIP6 ensemble whether these relationships could be improved and how they could be used, e.g., in impact models.

- Attribution studies of the FWI to anthropogenic climate change under historical and future projections. Heatwaves, droughts, and other extreme events have been attributed to climate change, but only limited studies have been able to attribute fires or mega-fires to climate change. The lack of relevant data explains this reduced number of attribution studies. Thanks to this provided dataset, attribution studies may use these data to assess changes in probabilities due to climate change. However, the provided dataset does not provide runs under the scenario "hist-nat", the historical run with only natural forcings but not anthropogenic forcings. It remains possible to use this dataset by considering the preindustrial period and current period with their corresponding natural variability.

- The FWI under CMIP5 and CMIP6. The FWI has been calculated for CMIP5 runs in Abatzoglou et al. (2019), while the provided dataset calculates the FWI for the latest CMIP6 exercise. A comparison of both datasets would allow us to identify changes in fire weather between the ESMs. Coupled to their respective burned areas, one may disentangle the causes of differences in fires under ESMs between the fire modules and fire weather of the models.

Appendix A

Table A1. List of the fire weather indices in the literature, extracted from the WSL (2022) (de Groot et al., 2015).

Fire Weather Index	Temperature	Rainfall	Relative humidity	Wind speed	Other	Reference
Munger					Days without rainfall	Munger (1916)
Nesterov	X				Days without rainfall	Nesterov (1949)
Angström	X		X			Chandler et al. (1983)
Zdhanko	X	X			Dew-point temperature	Zhdanko (1965)
GFDI	X		X	X	Fuel, grass condition	McArthur (1967)
FFDI	X		X	X	Fuel availability	McArthur (1967)
BI	X			X		Baumgartner (1967)
KBDI	X	X				Keetch and Byram (1968)
M68	X	X			Vegetation condition	Käse (1969)
Orieux	X	X		X		Orieux (1974)
FFWI	X	X	X		Drought index	Fosberg (1978)
NFDRS	X	X	X	X	Lightning, clouds	Deeming (1972)
EMC	X		X			Bradshaw et al. (1984)
LFDI	X		X			Meikle and Heine (1987)
FWI	X	X	X	X		Van Wagner (1987)
I87	X		X	X		Carrega (1991)
Haines index	X				Dew-point temperature	Haines et al. (1983)
Numerical risk	X		X	X	Cloud cover	Sol (1990)
Portuguese index	X	X		X	Dew-point temperature	Goncalves and Lourenco (1990)
F index	X		X	X		Sharples et al. (2009a, b)
FMI	X		X			Sharples et al. (2009a, b)
Fire danger	X	X	X			Setzer and Sismanoglu (2012)

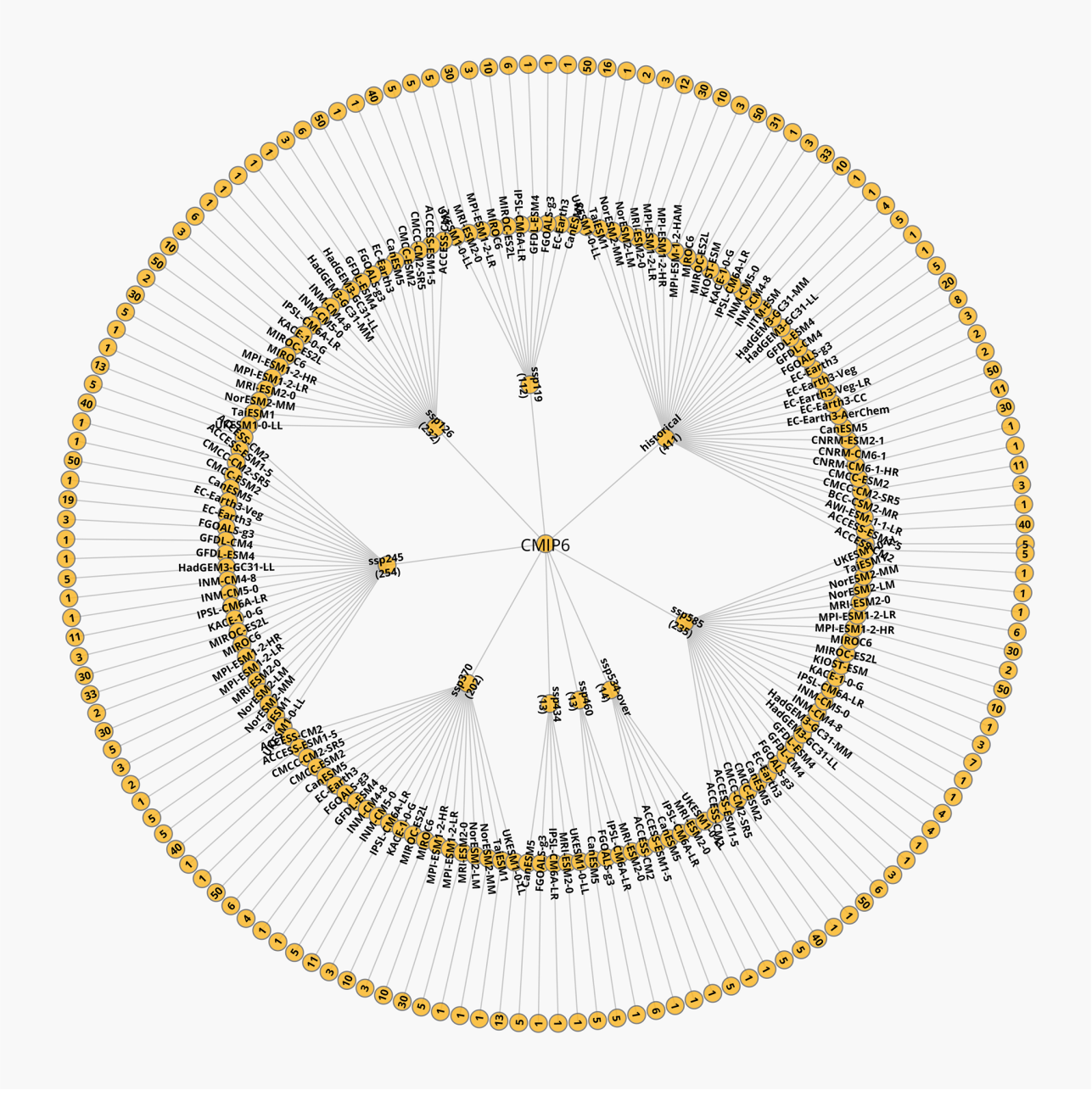

Figure A1. Same as Fig. 1 but with runs selected with daily average relative humidity (*hurs*) instead of daily minimum relative humidity (*hursmin*). Altogether, 1486 runs are presented here.

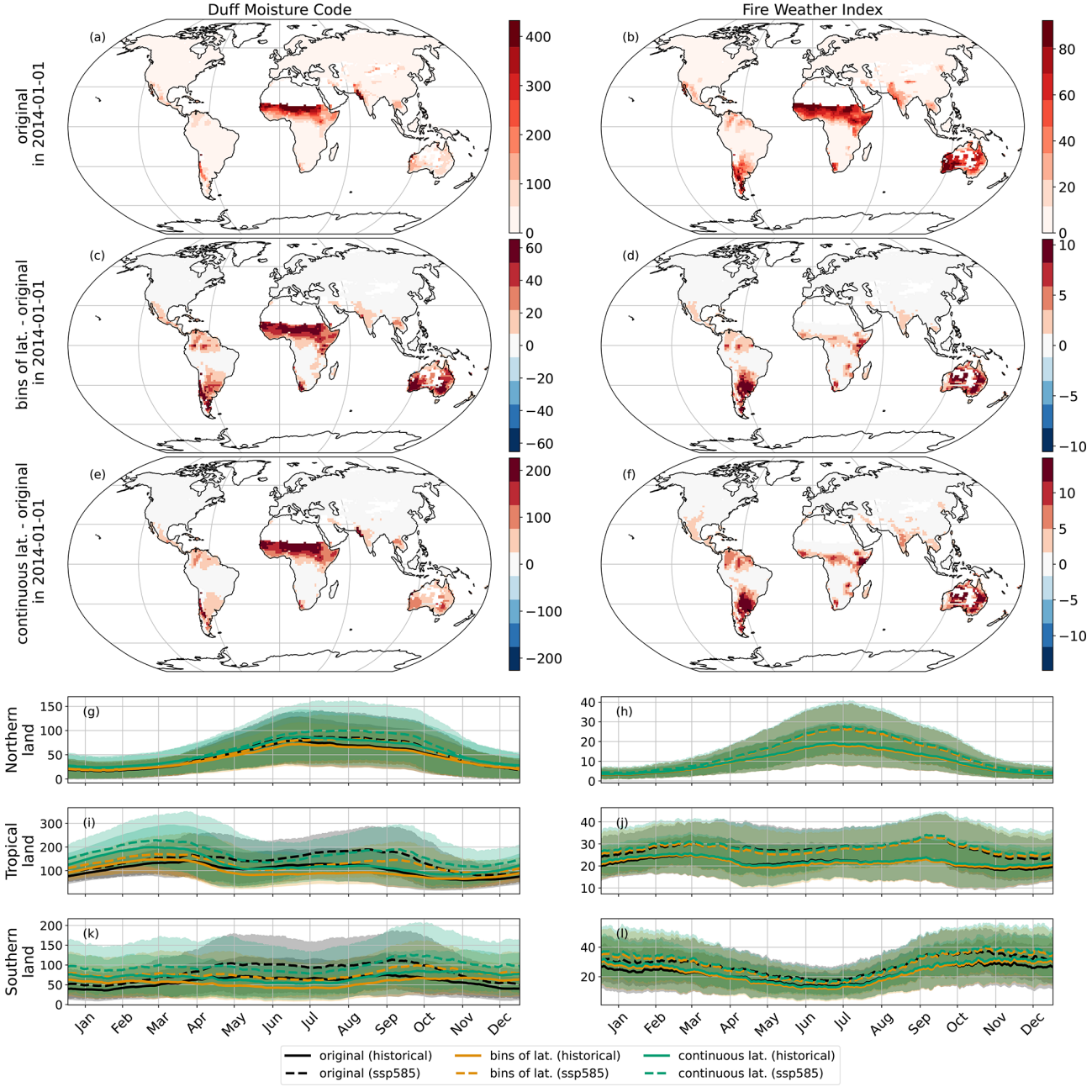

Figure A2. Similar to Fig. 3 but on 1 January 2014.

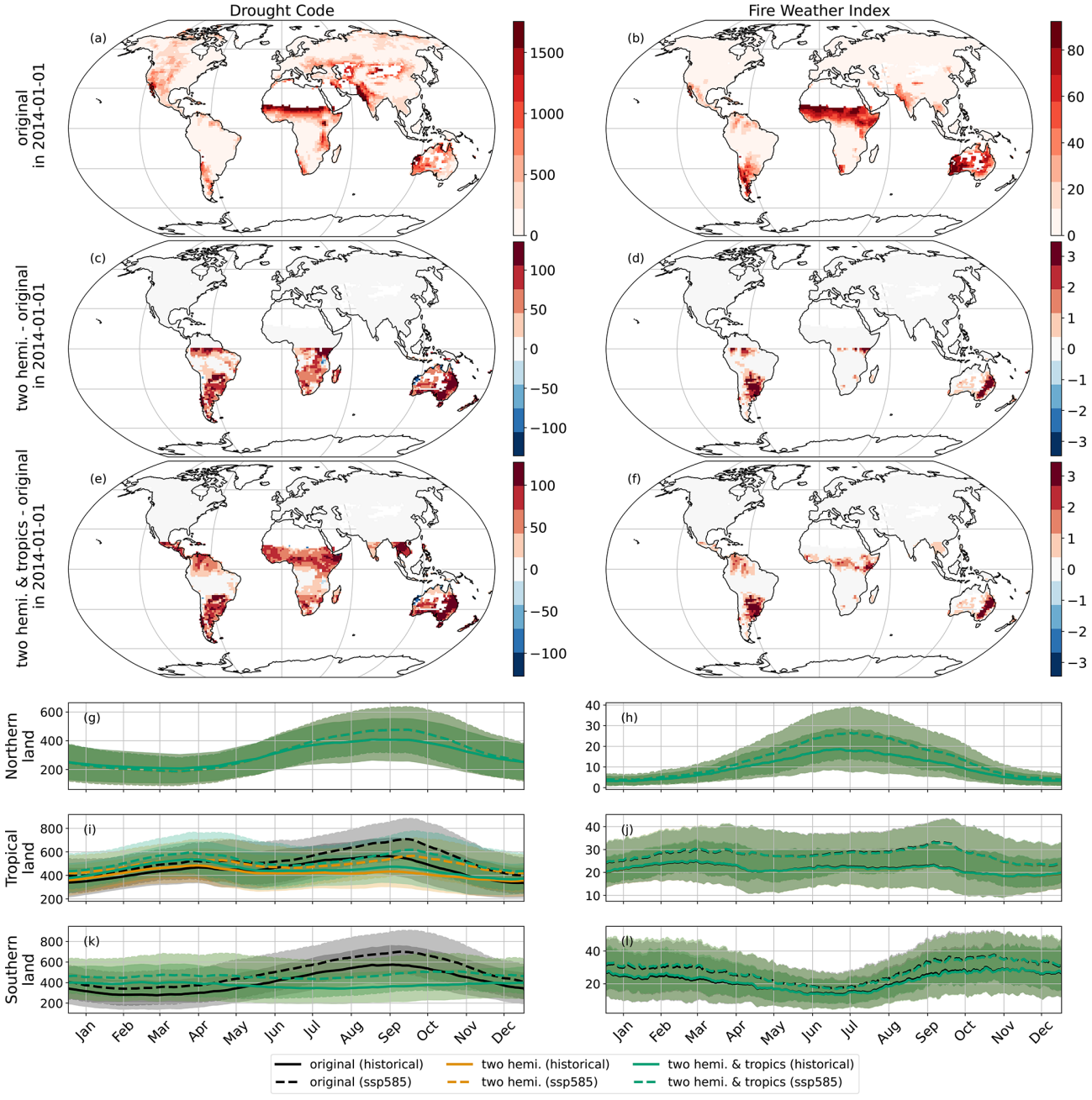

Figure A3. Similar to Fig. 4 but on 1 January 2014.

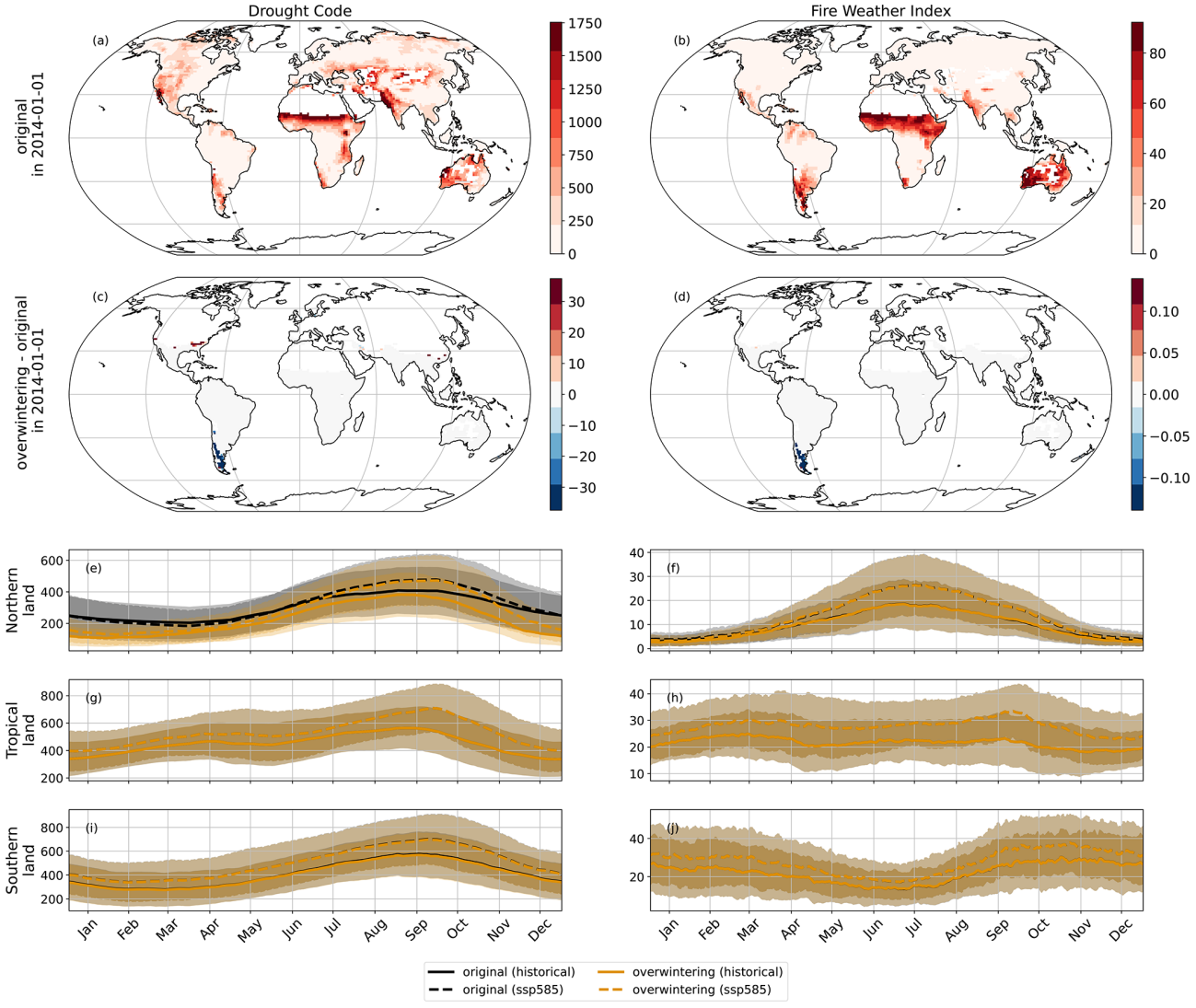

Figure A4. Similar to Fig. 5 but on 1 January 2014.

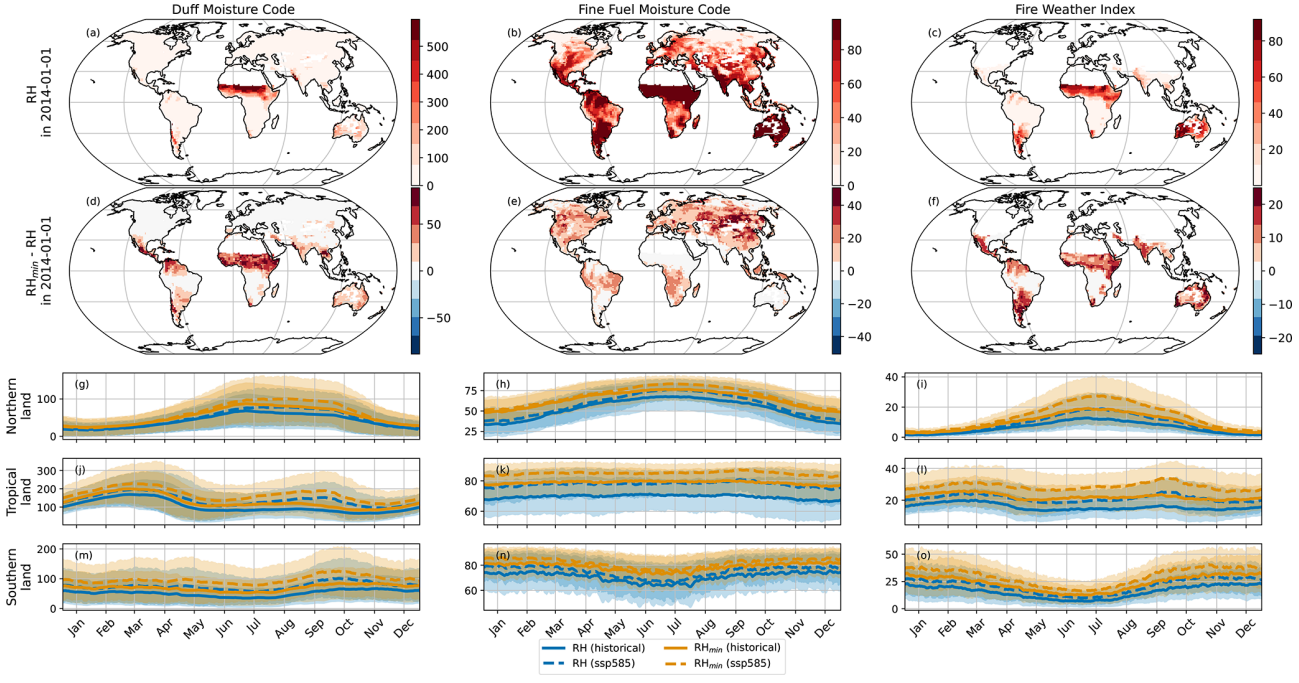

Figure A5. Similar to Fig. 6 but on 1 January 2014.

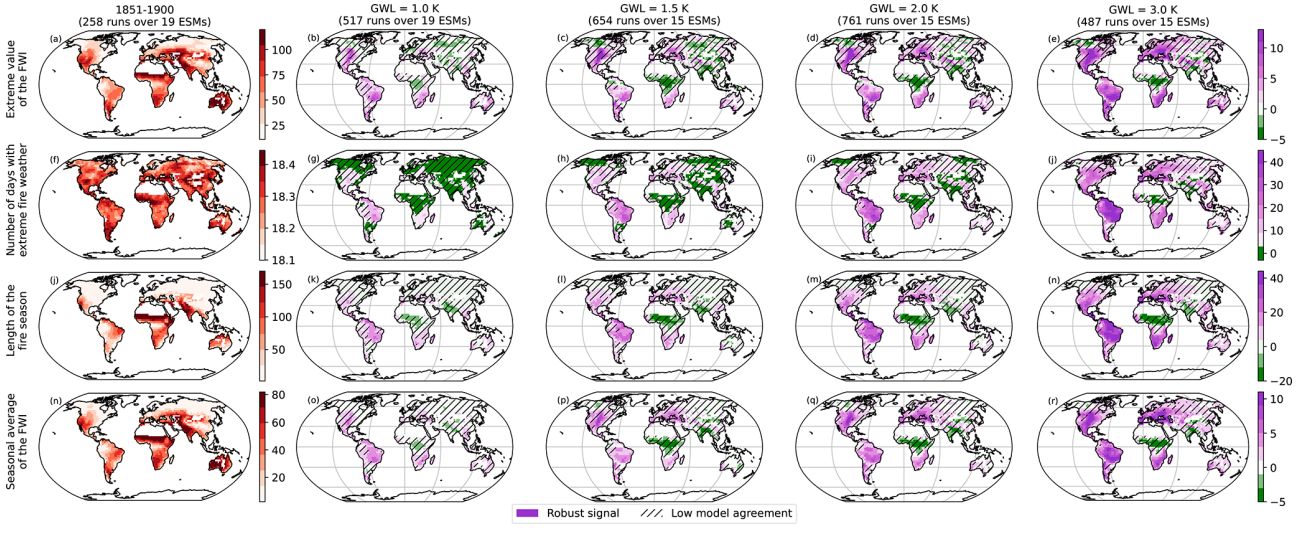

Figure A6. Similar to Fig. 7 but with no common subset for the selection of maps at different GWLs.

Method for global warming levels and uncertainties

Figures 7, 8, and A6 synthesize information on annual indicators of FWI by representing the maps at a specific global warming level (GWL) and then showing their robustness. The first step is the identification of the maps of annual indicators at each GWL.

1. With 1851–1900 as a reference period, we deduce the change in global mean surface temperature (*tas*) from each run used in this paper.
2. For a given GWL, we identify, for each run, whether the GWL is exceeded and its first year.
3. For each annual indicator, if a run has exceeded the GWL, we gather the maps of the indicator from the exceedance year -10 to the exceedance year $+9$.
4. If the run is a scenario with an exceedance year inferior or equal to 2023, the *historical period* is used to extend the missing year backwards.
5. If the run is *historical* and with an exceedance year superior or equal to 2005, *ssp245* is chosen to extend the missing year forwards. For this reason, only runs for which a corresponding *ssp245* has been run are selected.
6. For each run, the maps over this 20-year period are averaged to obtain the later Figs. 7 and A6. For Fig. 8, the 90th percentile is taken over this period.
7. We compile the ensemble of averaged maps reaching this GWL and proceed to map the robustness and uncertainties at each GWL.

We note that, the higher the GWL, the lower the number of runs reaching this GWL. This implies that the subset of runs used is different for each GWL. To avoid introducing a bias in the comparison, we choose to restrain the subset of runs to the runs that satisfy the higher represented GWL. This ensures the same subset of runs, although at the appropriate exceedance years. Because using this subset differs from the usual method, we have also added Fig. A.6, where the full set of runs respecting the GWL is used.

The former step provides us with a subset of maps at each GWL, coming from different runs and defined by the ESM, the scenario, and the ensemble member. This subset is averaged using the following method to avoid models with a higher number of scenarios or ensemble members being overrepresented. Model democracy is used here without discarding or weighting any model.

1. At each GWL, the subset of maps is first averaged over the ensemble members, not to give more weight to ESMs with large ensembles.
2. Afterwards, the subset of maps is averaged over the experiments, not to give more weight to ESMs that run more scenarios than others.
3. Finally, we average the ESMs.

We calculate the robustness of these maps following approach B of the IPCC (Gutiérrez et al., 2021), although the problem of overrepresentation of models had to be accounted for. Model democracy is also used here.

1. At each GWL, for each ESM, the maps for available scenarios and ensemble members are pooled.
2. If more than 80 % of these runs have the same sign for the evolution from the reference period, this ESM is marked as having a robust signal. As a note, the ensemble member and scenario dimensions are not differentiated here, so that enough runs are used to evaluate the robustness of the sign.
3. If more than 80 % of the ESMs at this GWL were marked as having a robust signal, then the signal is marked as overall robust.

Author contributions. YQ and FB performed FWI analyses with different methods in preparation for the manuscript and coordinated the present analyses. YQ merged the codes, computed the current database, and produced the figures and tables. YQ and FB jointly wrote the manuscript. All the authors co-designed the study, discussed the results, and contributed to the manuscript.

Competing interests. The contact author has declared that none of the authors has any competing interests.

Disclaimer. Publisher's note: Copernicus Publications remains neutral with regard to jurisdictional claims in published maps and institutional affiliations.

Acknowledgements. We thank the European Research Council (ERC) for ERC Proof Of Concept Grant MESMER-X (grant agreement no. 964013), project PROVIDE (grant agreement no. 101056875), and the Swiss National Science Foundation (SNSF) through the Compound Events in a Changing Climate (CECC) (grant agreement no. IZCOZ0_189941) project contributing to European COST Action CA17109, "Understanding and modeling compound climate and weather events" (DAMOCLES), which both funded this work, and project no. 186282, "Risk assessment of critical ecological thresholds in Amazonia and Cerrado". We thank the World Climate Research Program's Working Group on Coupled Modeling, which is responsible for the Coupled Model Intercomparison Project (CMIP), and we thank the climate modeling groups (listed in Fig. 1) for producing and making their model output available. Furthermore, we are indebted to Urs Beyerle, Lukas Brunner, and Ruth Lorenz for downloading and curating the CMIP6 data. We are also thankful to John Abatzoglou for pointing out the package cffdrs and the exchange on the FWI. Finally, we are thankful to Mathias Hauser for advice on how to curate the final products and regarding Figs. 7, 8, and A6.

Financial support. This research has been supported by the H2020 European Research Council (grant nos. 964013 and 101056875) and the Schweizerischer Nationalfonds zur Förderung der Wissenschaftlichen Forschung (grant nos. 189941 and 186282).

Review statement. This paper was edited by Dalei Hao and reviewed by three anonymous referees.

References

Abatzoglou, J. T., Williams, A. P., Boschetti, L., Zubkova, M., and Kolden, C. A.: Global patterns of interannual climate–fire relationships, Glob. Change Biol., 24, 5164–5175, https://doi.org/10.1111/gcb.14405, 2018.

Abatzoglou, J. T., Williams, A. P., and Barbero, R.: Global Emergence of Anthropogenic Climate Change in Fire Weather Indices, Geophys. Res. Lett., 46, 326–336, https://doi.org/10.1029/2018GL080959, 2019.

Agel, L. and Barlow, M.: How Well Do CMIP6 Historical Runs Match Observed Northeast U. S. Precipitation and Extreme Precipitation–Related Circulation?, J. Climate, 33, 9835–9848, https://doi.org/10.1175/JCLI-D-19-1025.1, 2020.

Ajibola, F. O., Zhou, B., Tchalim Gnitou, G., and Onyeju-ruwa, A.: Evaluation of the Performance of CMIP6 HighResMIP on West African Precipitation, Atmosphere, 11, 1053, https://doi.org/10.3390/atmos11101053, 2020.

Andela, N., Morton, D. C., Giglio, L., Chen, Y., van der Werf, G. R., Kasibhatla, P. S., DeFries, R. S., Collatz, G. J., Hantson, S., Kloster, S., Bachelet, D., Forrest, M., Lasslop, G., Li, F., Mangeon, S., Melton, J. R., Yue, C., and Randerson, J. T.: A human-driven decline in global burned area, Science, 356, 1356–1362, https://doi.org/10.1126/science.aal4108, 2017.

Anon: The complexities of wildfires, Nat. Geosci., 12, 81–81, https://doi.org/10.1038/s41561-019-0311-0, 2019.

Baumgartner, A.: Entwicklungslinien der forstlichen Meteorologie, Forstwiss. Centralbl., 86, 201–220, https://doi.org/10.1007/BF01821940, 1967.

Bedia, J., Herrera, S., Gutiérrez, J. M., Benali, A., Brands, S., Mota, B., and Moreno, J. M.: Global patterns in the sensitivity of burned area to fire-weather: Implications for climate change, Agr. Forest Meteorol., 214–215, 369–379, https://doi.org/10.1016/j.agrformet.2015.09.002, 2015.

Bedia, J., Golding, N., Casanueva, A., Iturbide, M., Buontempo, C., and Gutiérrez, J. M.: Seasonal predictions of Fire Weather Index: Paving the way for their operational applicability in Mediterranean Europe, Climate Services, 9, 101–110, https://doi.org/10.1016/j.cliser.2017.04.001, 2018.

Bowman, D. M. J. S., Williamson, G. J., Abatzoglou, J. T., Kolden, C. A., Cochrane, M. A., and Smith, A. M. S.: Human exposure and sensitivity to globally extreme wildfire events, Nat. Ecol. Evol., 1, 0058, https://doi.org/10.1038/s41559-016-0058, 2017.

Bradshaw, L. S., Deeming, J. E., Burgan, R. E., and Cohen, J. D.: The 1978 National Fire-Danger Rating System: technical documentation. General Technical Report INT-169, Ogden, UT: U.S. Department of Agriculture, Forest Service, Intermountain Forest and Range Experiment Station, 44 pp., https://doi.org/10.2737/INT-GTR-169, 1984.

Brunner, L., Hauser, M., Lorenz, R., and Beyerle, U.: The ETH Zurich CMIP6 next generation archive: technical documentation (v1.0-final), Zenodo, https://doi.org/10.5281/zenodo.3734128, 2020.

Carrega, P.: A Meteorological Index of Forest Fire Hazard in Mediterranean France, Int. J. Wildland Fire, 1, 79–86, https://doi.org/10.1071/WF9910079, 1991.

Carvalho, D., Cardoso Pereira, S., and Rocha, A.: Future surface temperatures over Europe according to CMIP6 climate projections: an analysis with original and bias-corrected data, Climatic Change, 167, 10, https://doi.org/10.1007/s10584-021-03159-0, 2021.

cffdrs: Canadian Forest Fire Danger Rating System, https://rdrr.io/rforge/cffdrs (last access: 11 October 2022), 2022.

Chandler, C., Cheney, P., Thomas, P., Trabaud, L., and Williams, D.: Fire in forestry. Volume 1. Forest fire behavior and effects. Volume 2. Forest fire management and organization, John Wiley & Sons, Inc., New York, xx + 450 pp.; xx + 298 pp., ISBN 0471874477, 1983.

daylight_fao56: https://www.ncl.ucar.edu/Document/Functions/Crop/daylight_fao56.shtml (last access: 11 October 2022), 2022.

de Groot, W. J., Field, R. D., Brady, M. A., Roswintiarti, O., and Mohamad, M.: Development of the Indonesian and Malaysian Fire Danger Rating Systems, Mitig. Adapt. Strat. Gl., 12, 165–180, https://doi.org/10.1007/s11027-006-9043-8, 2007.

de Groot, W. J., Wotton, B. M., and Flannigan, M. D.: Chapter 11 – Wildland Fire Danger Rating and Early Warning Systems, in: Wildfire Hazards, Risks and Disasters, edited by: Shroder, J. F. and Paton, D., Elsevier, Oxford, 207–228, https://doi.org/10.1016/B978-0-12-410434-1.00011-7, 2015.

Deeming, J. E.: The National Fire-Danger Rating System – 1978. Gen. Tech. Rep. INT-GTR-39. Ogden, UT: U.S. Department of Agriculture, Forest Service, Intermountain Forest and Range Experiment Station, 63 pp., 1972.

Douville, H., Qasmi, S., Ribes, A., and Bock, O.: Global warming at near-constant tropospheric relative humidity is supported by observations, Communications Earth & Environment, 3, 237, https://doi.org/10.1038/s43247-022-00561-z, 2022.

Dowdy, A. J., Mills, G. A., Finkele, K., and de Groot, W.: Index sensitivity analysis applied to the Canadian Forest Fire Weather Index and the McArthur Forest Fire Danger Index, Meteorol. Appl., 17, 298–312, https://doi.org/10.1002/met.170, 2010.

Dymond, C. C., Field, R. D., Roswintiarti, O., and Guswanto: Using Satellite Fire Detection to Calibrate Components of the Fire Weather Index System in Malaysia and Indonesia, Environ. Manage., 35, 426–440, https://doi.org/10.1007/s00267-003-0241-9, 2005.

ESA-CCI: Land Cover CCI Product User Guide Version 2, http://maps.elie.ucl.ac.be/CCI/viewer/download/ESACCI-LC-Ph2-PUGv2_2.0.pdf (last access: 25 May 2023), 2017.

ESA-CCI: New Release of the C3S Global Land Cover products for 2016, 2017 and 2018 consistent with the CCI 1992–2015 map series, https://www.esa-landcover-cci.org/?q=node/197 (last access: 11 October 2022), 2019.

Eyring, V., Bony, S., Meehl, G. A., Senior, C. A., Stevens, B., Stouffer, R. J., and Taylor, K. E.: Overview of the Coupled Model Intercomparison Project Phase 6 (CMIP6) experimen-

tal design and organization, Geosci. Model Dev., 9, 1937–1958, https://doi.org/10.5194/gmd-9-1937-2016, 2016.

Fan, X., Duan, Q., Shen, C., Wu, Y., and Xing, C.: Global surface air temperatures in CMIP6: historical performance and future changes, Environ. Res. Lett., 15, 104056, https://doi.org/10.1088/1748-9326/abb051, 2020.

Field, R. D.: Evaluation of Global Fire Weather Database reanalysis and short-term forecast products, Nat. Hazards Earth Syst. Sci., 20, 1123–1147, https://doi.org/10.5194/nhess-20-1123-2020, 2020.

Field, R. D., Spessa, A. C., Aziz, N. A., Camia, A., Cantin, A., Carr, R., de Groot, W. J., Dowdy, A. J., Flannigan, M. D., Manomaiphiboon, K., Pappenberger, F., Tanpipat, V., and Wang, X.: Development of a Global Fire Weather Database, Nat. Hazards Earth Syst. Sci., 15, 1407–1423, https://doi.org/10.5194/nhess-15-1407-2015, 2015.

Fosberg, M. A.: Weather in wildland fire management: the fire weather index, US For Serv Reprints of articles by FS employees, Environmental Science, 1978.

François, B., Vrac, M., Cannon, A. J., Robin, Y., and Allard, D.: Multivariate bias corrections of climate simulations: which benefits for which losses?, Earth Syst. Dynam., 11, 537–562, https://doi.org/10.5194/esd-11-537-2020, 2020.

Gallo, C., Eden, J. M., Dieppois, B., Drobyshev, I., Fulé, P. Z., San-Miguel-Ayanz, J., and Blackett, M.: Evaluation of CMIP6 model performances in simulating fire weather spatiotemporal variability on global and regional scales, Geosci. Model Dev. Discuss. [preprint], https://doi.org/10.5194/gmd-2022-223, in review, 2022.

Goncalves, Z. and Lourenco, L.: Meteorological index of forest fire risk in the Portuguese mainland territory, Proc Internat Conf Frest Fire Res, 1–14, 1990.

Grillakis, M., Voulgarakis, A., Rovithakis, A., Seiradakis, K. D., Koutroulis, A., Field, R. D., Kasoar, M., Papadopoulos, A., and Lazaridis, M.: Climate drivers of global wildfire burned area, Environ. Res. Lett., 17, 045021, https://doi.org/10.1088/1748-9326/ac5fa1, 2022.

Gutiérrez, J. M., Jones, R. G., Narisma, G. T., Alves, L. M., Amjad, M., Gorodetskaya, I. V., Grose, M., Klutse, N. A. B., Krakovska, S., Li, J., Martínez-Castro, D., Mearns, L. O., Mernild, S. H., Ngo-Duc, T., van den Hurk, B., and Yoon, J.-H.: Atlas, in: Climate Change 2021: The Physical Science Basis. Contribution of Working Group I to the Sixth Assessment Report of the Intergovernmental Panel on Climate Change, edited by: Masson-Delmotte, V., Zhai, P., Pirani, A., Connors, S., Péan, C., Berger, A., Caud, N., Chen, Y., Goldfarb, L., Gomis, M. I., Huang, M., Leitzell, K., Lonnoy, E., Matthews, J. B. R., Maycock, A., Waterfield, T., Yelekçi, O., Yu, R., and Zhou, B., Cambridge University Press, Cambridge, United Kingdom and New York, NY, USA, 1927–2058, https://doi.org/10.1017/9781009157896.021, 2021.

Haines, D. A., Main, W. A., Frost, J. S., and Simard, A. J.: Fire-Danger Rating and Wildfire Occurrence in the Northeastern United States, Forest Sci., 29, 679–696, 1983.

Jain, P., Tye, M. R., Paimazumder, D., and Flannigan, M.: Downscaling fire weather extremes from historical and projected climate models, Climatic Change, 163, 189–216, https://doi.org/10.1007/s10584-020-02865-5, 2020.

Jolly, W. M., Cochrane, M. A., Freeborn, P. H., Holden, Z. A., Brown, T. J., Williamson, G. J., and Bowman, D. M. J. S.: Climate-induced variations in global wildfire danger from 1979 to 2013, Nat. Commun., 6, 7537, https://doi.org/10.1038/ncomms8537, 2015.

Jones, P. W.: First- and Second-Order Conservative Remapping Schemes for Grids in Spherical Coordinates, Mon. Weather Rev., 127, 2204–2210, https://doi.org/10.1175/1520-0493(1999)127<2204:FASOCR>2.0.CO;2, 1999.

Jones, M. W., Abatzoglou, J. T., Veraverbeke, S., Andela, N., Lasslop, G., Forkel, M., Smith, A. J. P., Burton, C., Betts, R. A., van der Werf, G. R., Sitch, S., Canadell, J. G., Santín, C., Kolden, C., Doerr, S. H., and Le Quéré, C.: Global and Regional Trends and Drivers of Fire Under Climate Change, Rev. Geophys., 60, e2020RG000726, https://doi.org/10.1029/2020RG000726, 2022.

Käse, H.: Ein Vorschlag für eine Methode zur Bestimmung und Vorhersage der Waldbrandgefährdung mit Hilfe komplexer Kennziffern, 94, Akademie-Verlag, 1969.

Keetch, J. J. and Byram, G. M.: A drought index for forest fire control, US Department of Agriculture, Forest Service, Southeastern Forest Experiment Station, 35 pp., 1968.

Lasslop, G., Hantson, S., Harrison, S. P., Bachelet, D., Burton, C., Forkel, M., Forrest, M., Li, F., Melton, J. R., Yue, C., Archibald, S., Scheiter, S., Arneth, A., Hickler, T., and Sitch, S.: Global ecosystems and fire: Multi-model assessment of fire-induced tree-cover and carbon storage reduction, Glob. Change Biol., 26, 5027–5041, https://doi.org/10.1111/gcb.15160, 2020.

Lawson, B. D. and Armitage, O. B.: Weather Guide for the Canadian Forest Fire Danger Rating System, Natural Resources Canada Canadian Forest Service Northern Forestry Centre, ISBN 978-1-100-11565-8, 2008.

Li, F., Val Martin, M., Andreae, M. O., Arneth, A., Hantson, S., Kaiser, J. W., Lasslop, G., Yue, C., Bachelet, D., Forrest, M., Kluzek, E., Liu, X., Mangeon, S., Melton, J. R., Ward, D. S., Darmenov, A., Hickler, T., Ichoku, C., Magi, B. I., Sitch, S., van der Werf, G. R., Wiedinmyer, C., and Rabin, S. S.: Historical (1700–2012) global multi-model estimates of the fire emissions from the Fire Modeling Intercomparison Project (FireMIP), Atmos. Chem. Phys., 19, 12545–12567, https://doi.org/10.5194/acp-19-12545-2019, 2019.

Li, F., Zhang, X., and Kondragunta, S.: Highly anomalous fire emissions from the 2019–2020 Australian bushfires, Environmental Research Communications, 3, 105005, https://doi.org/10.1088/2515-7620/ac2e6f, 2021.

Libonati, R., Geirinhas, J. L., Silva, P. S., Monteiro dos Santos, D., Rodrigues, J. A., Russo, A., Peres, L. F., Narcizo, L., Gomes, M. E. R., Rodrigues, A. P., DaCamara, C. C., Pereira, J. M. C., and Trigo, R. M.: Drought–heatwave nexus in Brazil and related impacts on health and fires: A comprehensive review, Ann. N. Y. Acad. Sci., 2022, 1–31, https://doi.org/10.1111/nyas.14887, 2022.

Marlon, J. R., Bartlein, P. J., Walsh, M. K., Harrison, S. P., Brown, K. J., Edwards, M. E., Higuera, P. E., Power, M. J., Anderson, R. S., Briles, C., Brunelle, A., Carcaillet, C., Daniels, M., Hu, F. S., Lavoie, M., Long, C., Minckley, T., Richard, P. J. H., Scott, A. C., Shafer, D. S., Tinner, W., Umbanhowar, C. E., and Whitlock, C.: Wildfire responses to abrupt climate change in North America, P. Natl. Acad. Sci. USA, 106, 2519–2524, https://doi.org/10.1073/pnas.0808212106, 2009.

Martell, D. L.: A Markov chain model of day to day changes in the Canadian forest fire weather index, Int. J. Wildland Fire, 9, 265–273, 2000.

McArthur, A. G.: Fire behaviour in eucalypt forests, 1967.

McElhinny, M., Beckers, J. F., Hanes, C., Flannigan, M., and Jain, P.: A high-resolution reanalysis of global fire weather from 1979 to 2018 – overwintering the Drought Code, Earth Syst. Sci. Data, 12, 1823–1833, https://doi.org/10.5194/essd-12-1823-2020, 2020.

McKitrick, R. and Christy, J.: Pervasive Warming Bias in CMIP6 Tropospheric Layers, Earth and Space Science, 7, e2020EA001281, https://doi.org/10.1029/2020EA001281, 2020.

Meikle, S. and Heine, J.: A Fire Danger Index System for the Transvaal Lowveld and Adjoining Escarpment Areas, South African Forestry Journal, 143, 55–56, https://doi.org/10.1080/00382167.1987.9630304, 1987.

Munger, T. T.: GRAPHIC METHOD OF REPRESENTING AND COMPARING DROUGHT INTENSITIES, Mon. Weather Rev., 44, 642–643, https://doi.org/10.1175/1520-0493(1916)44<642:GMORAC>2.0.CO;2, 1916.

Natural Resources Canada: Background Information on the Canadian Forest Fire Weather Index (FWI) System, https://cwfis.cfs.nrcan.gc.ca/background/summary/fwi (last access: 11 October 2022), 2022.

NCAR/fire-indices: https://github.com/NCAR/fire-indices (last access: 11 October 2022), 2022.

Nesterov, V. G.: Forest Fire Danger and Methods of Its Determination, 1949 (in Russian).

O'Neill, B. C., Tebaldi, C., van Vuuren, D. P., Eyring, V., Friedlingstein, P., Hurtt, G., Knutti, R., Kriegler, E., Lamarque, J.-F., Lowe, J., Meehl, G. A., Moss, R., Riahi, K., and Sanderson, B. M.: The Scenario Model Intercomparison Project (ScenarioMIP) for CMIP6, Geosci. Model Dev., 9, 3461–3482, https://doi.org/10.5194/gmd-9-3461-2016, 2016.

Orieux, A.: Conditions météorologiques et incendies en région méditerranéenne, Revue forestière française, 26, 122–129, 1974.

Pfahl, S., O'Gorman, P. A., and Fischer, E. M.: Understanding the regional pattern of projected future changes in extreme precipitation, Nat. Clim. Change, 7, 423–427, https://doi.org/10.1038/nclimate3287, 2017.

pyfwi: https://github.com/buckinha/pyfwi (last access: 11 October 2022), 2022.

Quilcaille, Y. and Batibeniz, F.: Fire weather index data under historical and SSP projections in CMIP6 from 1850 to 2100, ETH Zurich [dataset], https://doi.org/10.3929/ethz-b-000583391, 2022.

Quilcaille, Y., Batibeniz, F., Ribeiro, A. F. S., Padrón, R. S., and Seneviratne, S. I.: Code associated with the publication "Fire weather index data under historical and SSP projections in CMIP6 from 1850 to 2100" (Version 1), Zenodo [code], https://doi.org/10.5281/zenodo.7971275, 2023.

Ranasinghe, R., Ruane, A. C., Vautard, R., Arnell, N., Coppola, E., Cruz, F. A., Dessai, S., Islam, A. S., Rahimi, M., Ruiz Carrascal, D., Sillmann, J., Sylla, M. B., Tebaldi, C., Wang, W., and Zaaboul, R.: Climate Change Information for Regional Impact and for Risk Assessment, in: Climate Change 2021: The Physical Science Basis. Contribution of Working Group I to the Sixth Assessment Report of the Intergovernmental Panel on Climate Change, edited by: Masson-Delmotte, V., Zhai, P., Pirani, A., Connors, S. L., Péan, C., Berger, S., Caud, N., Chen, Y., Goldfarb, L., Gomis, M. I., Huang, M., Leitzell, K., Lonnoy, E., Matthews, J. B. R., Maycock, T. K., Waterfield, T., Yelekçi, O., Yu, R., and Zhou, B., Cambridge University Press, Cambridge, United Kingdom and New York, NY, USA, 1767–1926, https://doi.org/10.1017/9781009157896.014, 2021.

Ribeiro, A. F. S., Brando, P. M., Santos, L., Rattis, L., Hirschi, M., Hauser, M., Seneviratne, S. I., and Zscheischler, J.: A compound event-oriented framework to tropical fire risk assessment in a changing climate, Environ. Res. Lett., 17, 065015, https://doi.org/10.1088/1748-9326/ac7342, 2022.

Rivera, J. A. and Arnould, G.: Evaluation of the ability of CMIP6 models to simulate precipitation over Southwestern South America: Climatic features and long-term trends (1901–2014), Atmos. Res., 241, 104953, https://doi.org/10.1016/j.atmosres.2020.104953, 2020.

Rossow, W. B., Mekonnen, A., Pearl, C., and Goncalves, W.: Tropical Precipitation Extremes, J. Climate, 26, 1457–1466, https://doi.org/10.1175/JCLI-D-11-00725.1, 2013.

San-Miguel-Ayanz, J., Durrant, T., Boca, R., Maianti, P., Libertá, G., Artés-Vivancos, T., Oom, D., Branco, A., de Rigo, D., Ferrari, D., Pfeiffer, H., Grecchi, R., and Nuijten, D.: Advance Report on Forest Fires in Europe, Middle East and North Africa 2021, Publications Office of the European Union, Luxembourg, https://doi.org/10.2760/039729, 2022.

Sanderson, B. M. and Fisher, R. A.: A fiery wake-up call for climate science, Nat. Clim. Change, 10, 175–177, https://doi.org/10.1038/s41558-020-0707-2, 2020.

Seneviratne, S. I., Zhang, X., Adnan, M., Badi, W., Dereczynski, C., Di Luca, A., Ghosh, S., Iskandar, I., Kossin, J., Lewis, S., Otto, F., Pinto, I., Satoh, M., Vicente-Serrano, S. M., Wehner, M., and Zhou, B.: Weather and Climate Extreme Events in a Changing Climate, in: Climate Change 2021: The Physical Science Basis. Contribution of Working Group I to the Sixth Assessment Report of the Intergovernmental Panel on Climate Change, edited by: Masson-Delmotte, V., Zhai, P., Pirani, A., Connors, S. L., Péan, C., Berger, S., Caud, N., Chen, Y., Goldfarb, L., Gomis, M. I., Huang, M., Leitzell, K., Lonnoy, E., Matthews, J. B. R., Maycock, T. K., Waterfield, T., Yelekçi, O., Yu, R., and Zhou, B., Cambridge University Press, https://doi.org/10.1017/9781009157896.013, 2021.

Setzer, A. and Sismanoglu, R.: Risco de fogo: metodologia do Cálculo: descrição sucinta da Versão 9, Instituto Nacional de Pesquisas Espaciais (INPE), https://queimadas.dgi.inpe.br/~rqueimadas/documentos/RiscoFogo_Sucinto_20130911.pdf (last access: 26 May 2023), 2012.

Sharples, J. J., McRae, R. H. D., Weber, R. O., and Gill, A. M.: A simple index for assessing fuel moisture content, Environ. Model. Softw., 24, 637–646, https://doi.org/10.1016/j.envsoft.2008.10.012, 2009a.

Sharples, J. J., McRae, R. H. D., Weber, R. O., and Gill, A. M.: A simple index for assessing fire danger rating, Environ. Model. Softw., 24, 764–774, https://doi.org/10.1016/j.envsoft.2008.11.004, 2009b.

Shen, C., Zha, J., Li, Z., Azorin-Molina, C., Deng, K., Minola, L., and Chen, D.: Evaluation of global terrestrial near-surface wind speed simulated by CMIP6 models and their future projections, Ann. N. Y. Acad. Sci., 1518, 249–263, https://doi.org/10.1111/nyas.14910, 2022.

Simard, A. J.: Computer Program to Calculate the Canadian Forest Fire Weather Index, Canadian Forestry Service, Ottawa, Ontario, 1970.

Sol, B.: Estimation du risque météorologique d'incendies de forêts dans le sud-est de la France, Revue forestière française, 42, 263–271, 1990.

Stevens-Rumann, C. S., Sieg, C. H., and Hunter, M. E.: Ten years after wildfires: How does varying tree mortality impact fire hazard and forest resiliency?, Forest Ecol. Manag., 267, 199–208, https://doi.org/10.1016/j.foreco.2011.12.003, 2012.

Tebaldi, C., Debeire, K., Eyring, V., Fischer, E., Fyfe, J., Friedlingstein, P., Knutti, R., Lowe, J., O'Neill, B., Sanderson, B., van Vuuren, D., Riahi, K., Meinshausen, M., Nicholls, Z., Tokarska, K. B., Hurtt, G., Kriegler, E., Lamarque, J.-F., Meehl, G., Moss, R., Bauer, S. E., Boucher, O., Brovkin, V., Byun, Y.-H., Dix, M., Gualdi, S., Guo, H., John, J. G., Kharin, S., Kim, Y., Koshiro, T., Ma, L., Olivié, D., Panickal, S., Qiao, F., Rong, X., Rosenbloom, N., Schupfner, M., Séférian, R., Sellar, A., Semmler, T., Shi, X., Song, Z., Steger, C., Stouffer, R., Swart, N., Tachiiri, K., Tang, Q., Tatebe, H., Voldoire, A., Volodin, E., Wyser, K., Xin, X., Yang, S., Yu, Y., and Ziehn, T.: Climate model projections from the Scenario Model Intercomparison Project (ScenarioMIP) of CMIP6, Earth Syst. Dynam., 12, 253–293, https://doi.org/10.5194/esd-12-253-2021, 2021.

Tian, X., McRae, D. J., Jin, J., Shu, L., Zhao, F., and Wang, M.: Wildfires and the Canadian Forest Fire Weather Index system for the Daxing'anling region of China, Int. J. Wildland Fire, 20, 963–973, https://doi.org/10.1071/WF09120, 2011.

van der Velde, I. R., van der Werf, G. R., Houweling, S., Maasakkers, J. D., Borsdorff, T., Landgraf, J., Tol, P., van Kempen, T. A., van Hees, R., Hoogeveen, R., Veefkind, J. P., and Aben, I.: Vast CO_2 release from Australian fires in 2019–2020 constrained by satellite, Nature, 597, 366–369, https://doi.org/10.1038/s41586-021-03712-y, 2021.

van Oldenborgh, G. J., Krikken, F., Lewis, S., Leach, N. J., Lehner, F., Saunders, K. R., van Weele, M., Haustein, K., Li, S., Wallom, D., Sparrow, S., Arrighi, J., Singh, R. K., van Aalst, M. K., Philip, S. Y., Vautard, R., and Otto, F. E. L.: Attribution of the Australian bushfire risk to anthropogenic climate change, Nat. Hazards Earth Syst. Sci., 21, 941–960, https://doi.org/10.5194/nhess-21-941-2021, 2021.

Van Wagner, C. E.: Development and structure of the Canadian forest fire weather index system, Canadian Forestry Service, Ottawa, 1987.

Varela, V., Sfetsos, A., Vlachogiannis, D., and Gounaris, N.: Fire Weather Index (FWI) classification for fire danger assessment applied in Greece, Journal of Mediterranean Meteorology & Climatology, 15, 31–40, https://doi.org/10.3369/tethys.2018.15.03, 2018.

Vitolo, C., Di Giuseppe, F., Krzeminski, B., and San-Miguel-Ayanz, J.: A 1980–2018 global fire danger re-analysis dataset for the Canadian Fire Weather Indices, Scientific Data, 6, 190032, https://doi.org/10.1038/sdata.2019.32, 2019.

Wang, Y., Anderson, K. R., and Suddaby, R. M.: Updated source code for calculating fire danger indices in the Canadian Forest Fire Weather Index System, Natural Resources Canada, Canadian Forest Service, Northern Forestry Centre, Edmonton, Alberta, 26, 2015.

Wilcox, E. M. and Donner, L. J.: The Frequency of Extreme Rain Events in Satellite Rain-Rate Estimates and an Atmospheric General Circulation Model, J. Climate, 20, 53–69, https://doi.org/10.1175/JCLI3987.1, 2007.

Wotton, B. M. and Flannigan, M. D.: Length of the fire season in a changing climate, Forest. Chron., 69, 187–192, https://doi.org/10.5558/tfc69187-2, 1993.

WSL: Fire Weather Indices WIKI, WSL, https://wikifire.wsl.ch/tiki-index4727.html?page=Indices&structure=Fire (last access: 11 October 2022), 2022.

Xu, Z., Han, Y., Tam, C.-Y., Yang, Z.-L., and Fu, C.: Bias-corrected CMIP6 global dataset for dynamical downscaling of the historical and future climate (1979–2100), Scientific Data, 8, 293, https://doi.org/10.1038/s41597-021-01079-3, 2021.

Zhdanko, V.: Scientific basis of development of regional scales and their importance for forest fire management, in: Contemporary Problems of Forest Protection from Fire and Firefighting, edited by: Melekhov, I. S., 53–89, 1965.